

ICARUS-TM/03-03
July 18, 2003

Oscillation effects on supernova neutrino rates and spectra and detection of the shock breakout in a liquid Argon TPC

I. GilBotella¹, A. Rubbia²

Institut für Teilchenphysik, ETH Z, CH-8093 Zurich, Switzerland

Abstract

A liquid Argon TPC (ICARUS-like) has the ability to detect clean neutrino bursts from type-II supernova collapses. In a previous paper we have considered three detection channels: elastic scattering on electrons from all neutrino species, e^- charged current absorption on Ar with production of excited K and e^- charged current absorption on Ar with production of excited Cl. In this paper, we study the effects of the three flavor neutrino oscillation on our analysis, including matter effects inside supernova. Results show a dramatic increase on the number of expected events due to oscillations and big changes in the energy spectrum, specially for charged-current events. We study the possibility to identify the mass hierarchy of neutrinos and to probe the neutrino oscillation parameter Δm^2_{13} by the observation of the neutrinos from the next galactic supernova. The shock breakout phase of pure emission of electron neutrinos has also been investigated using recent simulations of the core collapse supernova. A liquid Argon TPC is specially well suited for studying this signal since e^- charged current absorption on Ar with production of excited K can be well identified with the signature of associated photons from K de-excitation. For definiteness, the expected event rates and energy spectra are calculated for the 3 kton ICARUS detector. For the case of the shock breakout, we compare the event rates with those obtainable in SuperKamiokande and SNO.

¹ Ines.GilBotella@cern.ch

² Andre.Rubbia@cern.ch

1 Introduction

Core collapse supernovae are a huge source of all flavor neutrinos. Neutrino astrophysics entered a new phase with the detection of neutrinos from the supernova SN 1987A in the Large Magellanic Cloud by the Kamiokande and IMB detectors [1]. In spite of these fundamental neutrino observations, the 19 events observed are not statistically significant enough to obtain quantitative information on the neutrino spectrum. New neutrino detectors have now the capabilities to provide high statistics information about supernova and neutrino properties if a supernova collapse were to take place in the near future.

The neutrino signal from a galactic supernova can give information about the intrinsic properties of the neutrino such as mass and flavor oscillation. In particular, the neutrino absolute mass can be investigated from measurements of the time of light delay and neutrino oscillations (flavor conversion in supernova core, in Earth) from the neutrino energy spectra. But also the core collapse physics can be studied. The flavor composition, energy spectrum and time structure of the neutrino burst will yield information on the explosion mechanism and the mechanisms of proto neutron star cooling. Finally, because neutrinos arrive before any other signal from a supernova, it is possible to provide an early alert to the astronomical community combining the observations of several experiments. This will allow an early observation of the first stages of the supernova explosion.

Although new oscillation data from solar, atmospheric, reactor and accelerator neutrinos [2] have contributed to the understanding of the neutrino properties, still the neutrino mixing angle θ_{13} and the nature of the mass hierarchy, i.e., normal or inverted, remain unknown. These parameters can be probed by the observation of supernovae neutrino bursts, since neutrinos will travel long distances before reaching the Earth and will in addition traverse regions of different matter density where matter enhanced oscillations will take place. In the case of the θ_{13} angle, matter enhancement has the striking feature that very small mixing angles, well beyond any value detectable by next generation accelerators, could in fact alter significantly the neutrino spectrum. Hence, supernova neutrinos provide indeed a complementary tool to study the θ_{13} angle.

In this work we study the capabilities of a liquid Argon TPC (ICARUS-like) to detect neutrinos from supernova collapses and its possible contributions to this field. We have already computed the expected rates for supernova neutrinos in such a detector without considering neutrino oscillation effects [3]. New calculations on the cross section for the absorption processes based in the random phase approximation (RPA) were used allowing computing for the first time the contribution of the $e^- + {}^{40}Ar \rightarrow e^- + {}^{40}Ar$ absorption reaction. The elastic scattering neutrino events have let us reconstruct the supernova direction with good accuracy by measuring the direction of the lepton momentum.

But neutrino oscillations will modify significantly the expected neutrino rates and energy distributions. Since the average neutrino energy is flavor dependent ($E_{\nu_e} < E_{\nu_\mu} < E_{\nu_\tau}$), neutrino oscillations make the spectra of ν_μ and ν_τ harder. This will lead to a big change in the neutrino observations in the detector because the cross sections

depend strongly on the neutrino energy and they are different for different flavor.

In this note we include the effects of neutrino oscillations in vacuum and in the supernova matter and we compute the expected neutrino rates in a liquid Argon TPC. For definiteness, the expected event rates and energy spectra are calculated for the 3 kton ICARUS detector[4]. Moreover, the energy spectra modified by oscillations are plotted for different conditions on the oscillation parameters. From supernova neutrino observations it is possible to extract information about the character of the mass hierarchy and the $_{13}$ mixing angle.

Particular interest is taken on the early phase neutrino signal from supernova. We investigate the expected events coming from the first milliseconds after the supernova bounce using the latest calculations on the shock breakout process in core collapse supernovae and taking neutrino oscillations into account.

1.1 General framework

In this note we analyze in detail the signatures of neutrinos from stellar collapses. The following general considerations are taken in the present analysis:

SN type-II at a distance of 10 kpc (galactic supernovae) are studied.

Gravitational binding energy of 3×10^{53} ergs. Almost all of this binding energy is radiated away as neutrinos.

From the neutrino emission point of view, we consider two phases: the early pulse expected in the first 40 ms of the collapse (shock breakout) and the cooling stage, with the emission of all flavor neutrinos. The expected time for the whole neutrino emission is 10 s.

For the cooling stage we assume that the energy spectra of neutrinos is a Fermi-Dirac distribution and that the total luminosity is equally shared by all flavors.

The most commonly assumed neutrino average energies are:

$$\bar{E}_e = 11 \text{ MeV}, \bar{E}_\mu = 16 \text{ MeV}, \bar{E}_\tau = 25 \text{ MeV}$$

Normal ($m_1^2 < m_2^2 < m_3^2$) and inverted ($m_3^2 < m_1^2 < m_2^2$) mass hierarchies are investigated in the analysis.

Matter effects inside the supernova are included.

The following neutrino oscillations parameters are used in the analysis, obtained from other neutrino observations [2]:

$$\begin{aligned} \sin^2 2\beta_{23} &= 1: & m_{32}^2 &= 3 \times 10^{-3} \text{ eV}^2 \\ \sin^2 \theta_{12} &= 0.3: & m_{21}^2 &= 7 \times 10^{-5} \text{ eV}^2 \\ \sin^2 \theta_{13} &< 0.2 \end{aligned} \tag{1}$$

The mass of the planned 3kton ICARUS detector[4] is considered for the calculations.

2 Core collapse supernovae

When the iron core of a massive star ($M = 8 M_{\odot}$) overcomes its hydrodynamical stability limit (the Chandrasekhar mass), the core collapses raising its density up to many times the nuclear density. During this infall stage of the collapse, a first e^- burst is emitted ("infall burst"), since the high density of matter enhances the electron capture by protons. The total energy radiated during this phase is roughly 10^{51} ergs.

This emission does not continue indefinitely, since at a density $10^{12} \text{ g cm}^{-3}$ neutrinos are trapped in the stellar core and go to equilibrium with matter. The anomalous density produces an elastic bounce of the core, which results in a shock wave. After the core bounce, also neutrinos of other flavors begin to be produced. The neutrinos are trapped in a region ("neutrinosphere") whose size is different for different neutrino flavors. A deeper neutrinosphere corresponds to a higher temperature.

The wave propagates through the star and loses energy in dissociating nucleons. When the shock crosses the e^- neutrinosphere, an intense burst of e^- ("shock breakout" or "neutronization burst") is produced by electron capture on the large number of protons liberated by the shock. The characteristic time of the breakout burst is $3 \pm 10 \text{ ms}$ and the total energy radiated in e^- neutrinos during breakout is 3 ± 10^{51} ergs. A liquid Argon TPC is specially well suited for studying this signal since e^- charged current absorption on Argon with production of excited K^- can be well identified with the signature of associated photons from K^- de-excitation.

After the breakout stage, the e^- luminosity rapidly decreases, while the luminosities of other flavor neutrinos increase. At the end of the neutrino diffusion inside the mantle the energy is practically equally distributed between the various neutrino flavors. The star loses energy, mainly by neutrino emission, and cools down, forming a neutron star or a black hole. This final stage ("cooling") requires 10 s and takes away $> 99\%$ of the gravitational energy of the star ($2 \pm 4 \times 10^{53}$ ergs). A liquid Argon TPC can detect all neutrino flavors through elastic scattering on electrons $e^- + e^- \rightarrow e^- + e^-$, and distinguish the fluxes of e^- and e^+ through charged-current (CC) interactions on argon $e^- + ^{40}\text{Ar} \rightarrow e^- + ^{40}\text{K}^- + ^{40}\text{Ar} \rightarrow e^+ + ^{40}\text{Cl}$. There is a possibility to separate the two last channels by a classification of the associated photons from the K^- or Cl de-excitation, which exhibit specific lines.

3 Neutrino oscillations and matter effects

Neutrinos produced in the high density region of the iron core interact with matter before emerging from the supernova. Due to the non-zero masses and non-zero vacuum mixing angles among various neutrino flavors, flavor conversions can occur in supernovae.

The transitions are produced mainly in the so-called resonance layers. The resonance density is given by [5]:

$$_{\text{res}} = \frac{1}{2} \frac{p}{2G_F} \frac{m^2 m_N}{E} \frac{Y_e}{Y_e} \cos 2\theta$$
(2)

where G_F is the Fermi constant, m^2 is the mass squared difference, θ is the mixing angle, E is the neutrino energy, m_N is the nucleon mass and Y_e is the number of electrons per nucleon.

Since the inner supernova core is too dense to allow resonance conversion, we can consider two resonance points in the outer supernova envelope: one at high density $10^3 \{ 10^4 \text{ g cm}^{-3}$ (H resonance) which is governed by the atmospheric parameters (m_{31}^2 and $_{13}$) and the other one at low density $10 \{ 30 \text{ g cm}^{-3}$ (L resonance), characterized by the solar parameters (m_{21}^2 and $_{12}$).

The transitions in the two resonance layers can be considered independently and each transition is reduced to a two neutrino oscillation problem. The H resonance lies in the neutrino channel for normal mass hierarchy and in the antineutrino channel for the inverted hierarchy. The L resonance lies in the neutrino channel for both the hierarchies [5].

The probability of transition between one neutrino eigenstate to another in the resonance layer (L or H) is called jump probability (P_L or P_H).

The propagation through the low density region is always adiabatic for the LMA solar parameters. It means that P_L and \bar{P}_L are both equal to 0 and the neutrino mass eigenstates remain unchanged.

Considering a matter density profile of the star $(r) / r^3$, the jump probability in the H resonance can be written as [5]:

$$P_H / \exp^4 \text{ const} \sin^2 _{13} \frac{m_{31}^2 \theta_{2=3}^3}{E^5}$$
(3)

Indeed, the neutrino conversion in the high density region depends on the mixing angle $_{13}$ and the mass squared difference between the involved flavors, as shown in figure 1. The variation of the jump probability with the $_{13}$ -mixing angle and the neutrino energy is plotted. We see that the crossing probability increases with energy. Three regions can be distinguished:

1. Non adiabatic region ($\sin^2 _{13} < 2 \cdot 10^{-6}$): For these values of $_{13}$ the jump probability is almost equal to 1, independently of the neutrino energy.
2. Intermediate region ($2 \cdot 10^{-6} < \sin^2 _{13} < 3 \cdot 10^{-4}$): In this region the value of P_H , between 0 and 1, depends on $_{13}$ and neutrino energy as expressed in the equation 3.
3. Adiabatic region ($\sin^2 _{13} > 3 \cdot 10^{-4}$): The jump probability is equal to 0 for any value of the neutrino energy. Then, there is no conversion between eigenstates in the resonance layer.

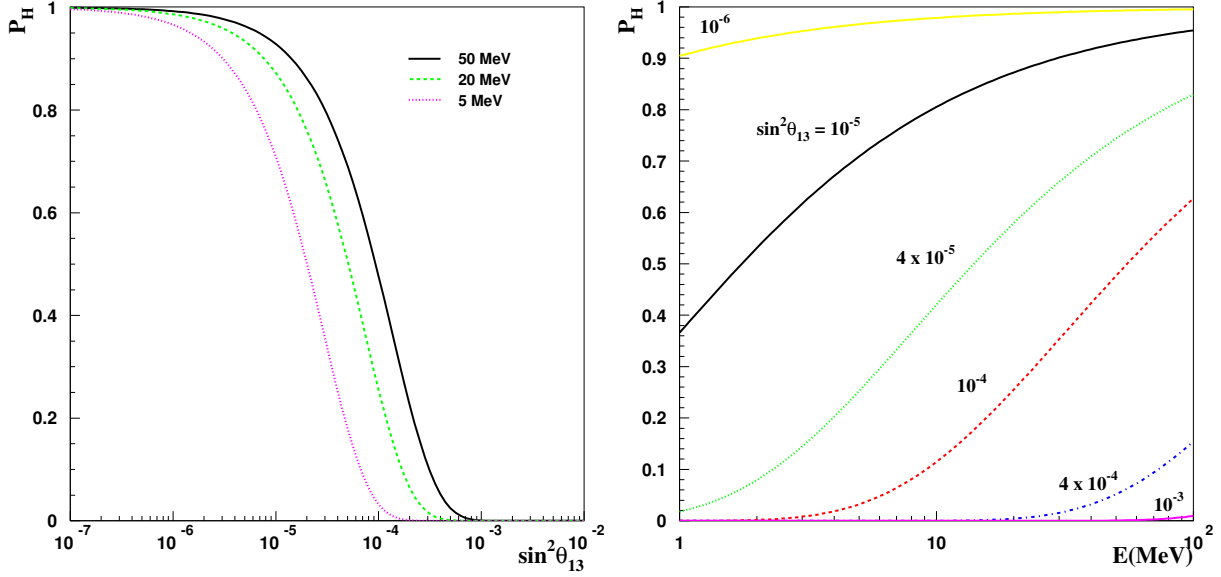


Figure 1: Jump probability in the H-resonance, P_H , as a function of $\sin^2 \theta_{13}$ for three values of the neutrino energy (left), and as a function of the neutrino energy for different values of $\sin^2 \theta_{13}$ (right).

The effect of oscillations in the neutrino fluxes is summarized in equation 4, where the expected fluxes at the detector (\circ) are computed in terms of the original fluxes at the SN core (\circ) and the survival probabilities $P_{ee} = P(e \rightarrow e)$ and $\bar{P}_{ee} = P(e \rightarrow \bar{e})$ ¹:

$$\begin{aligned} e &= \circ_e P_{ee} + \circ_x (1 - P_{ee}) \\ \bar{e} &= \circ_e \bar{P}_{ee} + \circ_x (1 - \bar{P}_{ee}) \\ + &= \circ_e (1 - P_{ee}) + \circ_x (1 + P_{ee}) \\ + &= \circ_e (1 - \bar{P}_{ee}) + \circ_x (1 + \bar{P}_{ee}) \end{aligned} \quad (4)$$

with $\circ_x = \circ = \circ = \circ_x = \circ = \circ$. If the original fluxes were equal between flavors, any oscillation effect could be observed.

The survival probabilities can be written in terms of jump probabilities as [5]:

$$\begin{aligned} P_{ee} &= P_H P_L \bar{J}_{e1} \bar{J} + P_H (1 - P_L) \bar{J}_{e2} \bar{J} + (1 - P_H) \bar{J}_{e3} \bar{J} \\ \bar{P}_{ee} &= (1 - P_L) \bar{J}_{e1} \bar{J} + P_L P_H \bar{J}_{e2} \bar{J} \end{aligned} \quad (5)$$

for normal hierarchy ($m_{32}^2 > 0$) and

$$\begin{aligned} P_{ee} &= P_L \bar{J}_{e1} \bar{J} + (1 - P_L) \bar{J}_{e2} \bar{J} \\ \bar{P}_{ee} &= P_H (1 - P_L) \bar{J}_{e1} \bar{J} + \bar{P}_L P_H \bar{J}_{e2} \bar{J} + (1 - P_H) \bar{J}_{e3} \bar{J} \end{aligned} \quad (6)$$

for inverted hierarchy ($m_{32}^2 < 0$).

¹We neglect the possible effect of the propagation through the mass of the Earth.

Considering the values of the $\sin^2 \theta_{13}$ probabilities and using the standard parametrization of the mixing matrix, the survival probabilities can be computed as shown in figure 2. The evolution of the probability P_{ee} (\bar{P}_{ee}) that a neutrino emitted as e^- (e^-) at the neutrinosphere remains as e^- (e^-) at Earth is plotted as a function of the θ_{13} mixing angle for different values of neutrino energy.

The upper plot corresponds to the normal hierarchy case (n.h.) and the lower one to the inverted hierarchy (i.h.). For n.h., the survival probability in the antineutrino channel does not depend on the neutrino energy and only very weakly on θ_{13} . However, the neutrino channel is very sensitive to θ_{13} via the P_H parameter. For inverted hierarchy the neutrino channel is independent on θ_{13} while the antineutrino channel depends on the θ_{13} mixing angle and neutrino energy.

According to the adiabaticity conditions in the H resonance and the value of the θ_{13} angle, three regions can be distinguished. If energy spectra are different, then θ_{13} and the mass hierarchy can be probed as follows:

For small mixing angle ($\sin^2 \theta_{13} < 2 \cdot 10^{-6}$), there are no effects on θ_{13} and both hierarchies give similar results. Therefore, in this region we can not distinguish among hierarchies and only an upper bound on $\sin^2 \theta_{13}$ can be set.

For intermediate θ_{13} ($2 \cdot 10^{-6} < \sin^2 \theta_{13} < 3 \cdot 10^{-4}$) maximal sensitivity to the angle is achieved and measurements of the angle are possible in this region.

For large mixing angle ($\sin^2 \theta_{13} > 3 \cdot 10^{-4}$) maximal conversions occur. The effect of the mixing is strong in neutrino (antineutrino) channel if the mass hierarchy is normal (inverted). We are able to probe the mass hierarchy in this region but only a lower bound on θ_{13} can be put.

4 Expected supernova neutrino signal

A liquid Argon TPC has the ability to detect clean neutrino bursts from type-II supernova collapses. In our previous paper [3], we have considered three detection channels: elastic scattering on electrons from all neutrino species, e^- charged current absorption on Ar with production of excited K and e^- charged current absorption on Ar with production of excited Cl. Thanks to its high sensitivity to e^- neutrinos, a liquid Argon TPC can observe and uniquely identify the electron neutrino breakout burst. For the 3kton ICARUS detector, the rates are such that one is able to detect neutrinos coming from galactic supernovas.

The three main channels of neutrino detection are

(1) elastic scattering on electrons

$$e^- + e^- \rightarrow e^- + e^- \quad (7)$$

(2) charged-current (CC) interactions on argon

$$e^- + {}^{40}\text{Ar} \rightarrow e^- + {}^{40}\text{K} \quad (8)$$

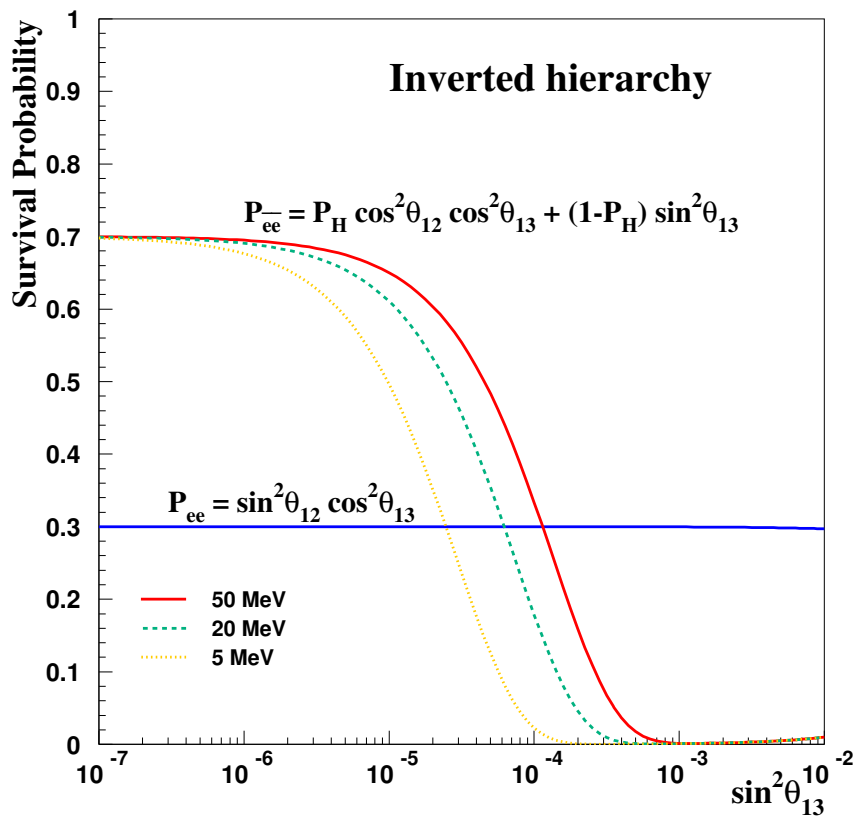
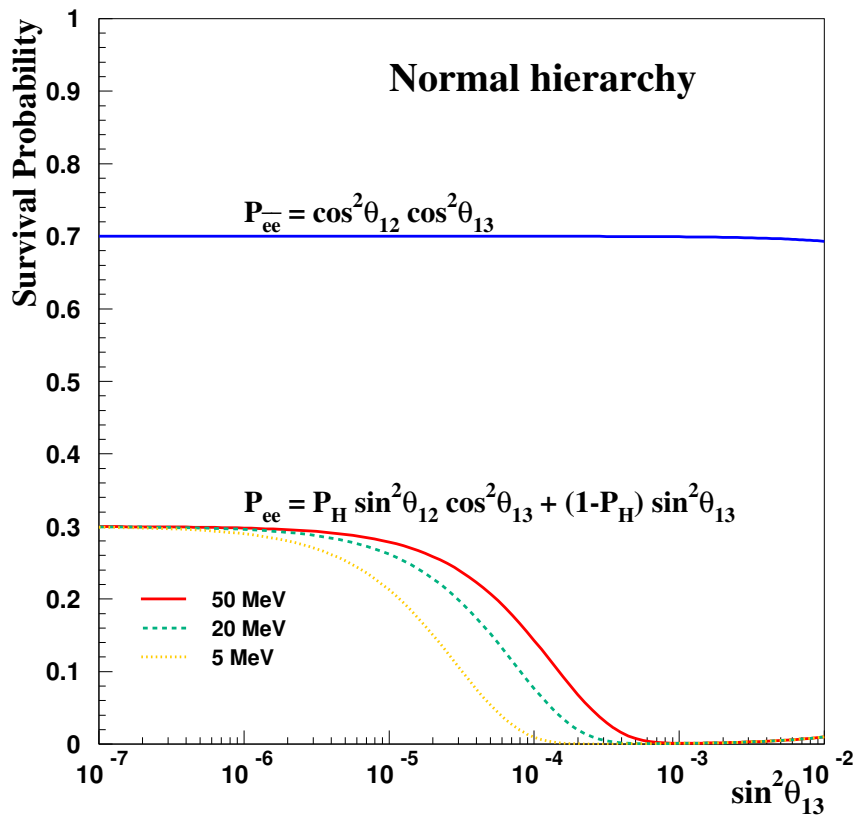


Figure 2: Survival probabilities for normal (top) and inverted (bottom) hierarchies as a function of $\sin^2 \theta_{13}$ and different values of neutrino energies.



The first reaction involves all neutrino flavors while the CC reactions (8 and 9) are only sensitive for electron neutrino and antineutrino. The Q value of the e^- CC process is 1.5 MeV while for the e^+ CC case is 7.48 MeV. The cross sections used for all these processes are already described in [3].

The differential number of neutrinos detected at a distance D from the supernova can be computed as:

$$dN_{\text{events}} = \frac{N_{\text{targets}}}{4 \pi D^2} \frac{dN}{dE \ dt} (\langle E \rangle) dE \ dt \quad (10)$$

where N_{targets} is the number of targets, D is the supernova distance (we assume $D = 10$ kpc for a typical galactic supernova), E is the neutrino energy, t is the detector time, $dN = dE \ dt$ is the time and energy spectra of the neutrinos and $\langle E \rangle$ is the cross section of a given process.

For the neutrino breakout phase the explicit neutrino flux distributions $dN = dE \ dt$ are taken from the calculations in [6]. Recent studies on the initial mass progenitor dependence seem to indicate that the major features of the early neutrino burst are almost independent of the initial mass of the star [7].

For the cooling phase, we assume a Fermi-Dirac distribution (see [3] for more details).

5 Supernova collapse and neutrino breakout phase

The neutrino shock breakout burst is the signal event in the supernova core collapse evolution. Its detection and characterization could test fundamental aspects of the current collapse supernova paradigm. The prompt electron neutrino burst is in principle observable and represents a diagnostic of the fundamental collapse supernova behavior. The characteristic time of the breakout burst is $\sim 3\{10$ ms.

The advantage of the early phase analysis is that it should not be affected by the time evolution of the density structure of the star nor whether the remnant is a neutron star or a black hole (see e.g. [6]). The shock wave takes about 2 seconds to reach the H-resonance region. Therefore, the potential time dependence of neutrino oscillations due to shock propagation can be neglected in the early phase.

Figure 3 shows the time evolution of the neutrino luminosities in the early phase of neutrino burst reconstructed from the simulation in [6]. The different neutrino flavors produced at different moments of the evolution are included in the picture. The time origin is arbitrary and the supernova core bounce time is set to $t = 0.2$ s. This time is taken as the reference for the rest of the processes. The calculation is based on dynamical models of core collapse supernovae in one spatial dimension, employing a newly-developed Boltzmann neutrino radiation transport algorithm, coupled to Newtonian Lagrangean hydrodynamics and a consistent high-density nuclear equation of state. Full details of the simulation can be found in [6].

The energy spectra of the different neutrino flavours is predicted to change with time. Figure 4 shows the particular energy distribution at 100 ms after the shock breakout.

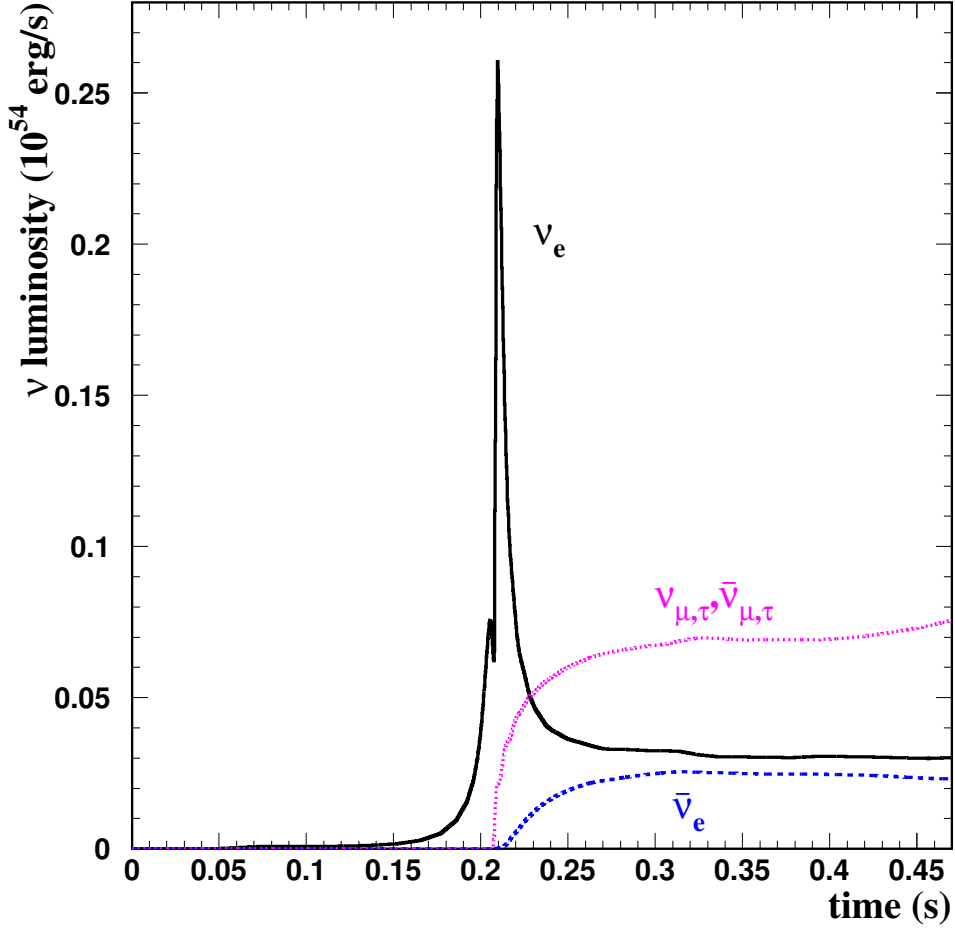


Figure 3: Time evolution of the ν_e (solid line), $\bar{\nu}_e$ (dashed line) and $\nu_{\mu,\tau}, \bar{\nu}_{\mu,\tau}$ (dotted line) neutrino luminosities due to a neutrino burst from a supernova at a distance of 10 kpc. The time origin is arbitrary and the shock breakout occurs at 0.2 s.

Figure 5 shows the time evolution of the neutrino flux for the different flavours expected at Earth coming from the supernova burst. The figure on the right corresponds to the time-integrated energy spectrum of the first 470 ms. The main contribution comes from the ν_e emission due to the supernova shock breakout.

The evolution of the expected event rates in the 3 kton ICARUS detector is shown in Figure 6 for the case of no oscillations. The contribution of ν_e events from the burst, including elastic and CC events (dark region), is separated from the rest of the flavor processes (light region). Note the small contribution of these flavours to the total rate.

A liquid Argon TPC has an excellent sensitivity to ν_e neutrinos mainly through the

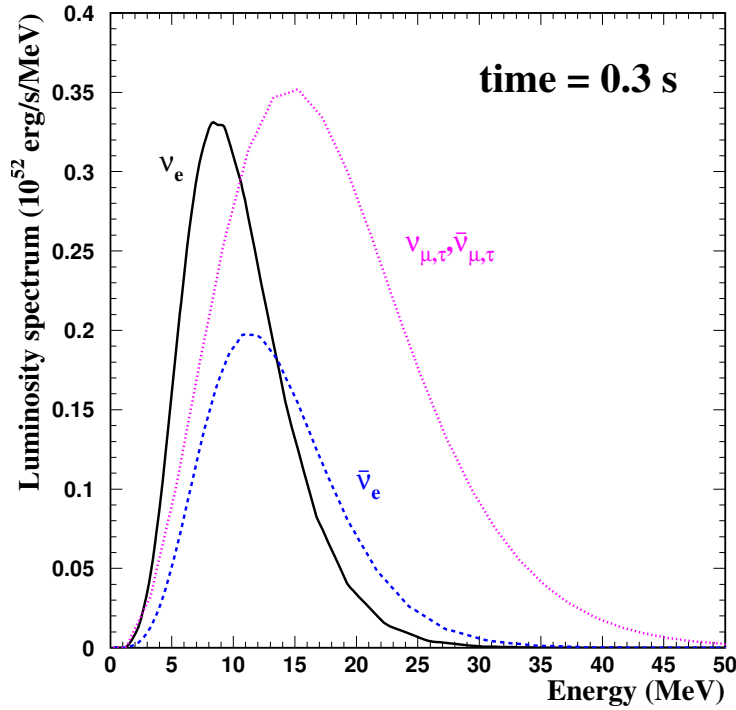


Figure 4: Luminosity spectrum of ν_e (solid line), $\bar{\nu}_e$ (dashed line) and $\nu_{\mu,\tau}, \bar{\nu}_{\mu,\tau}$ (dotted line) neutrinos at 100 ms after the shock breakout.

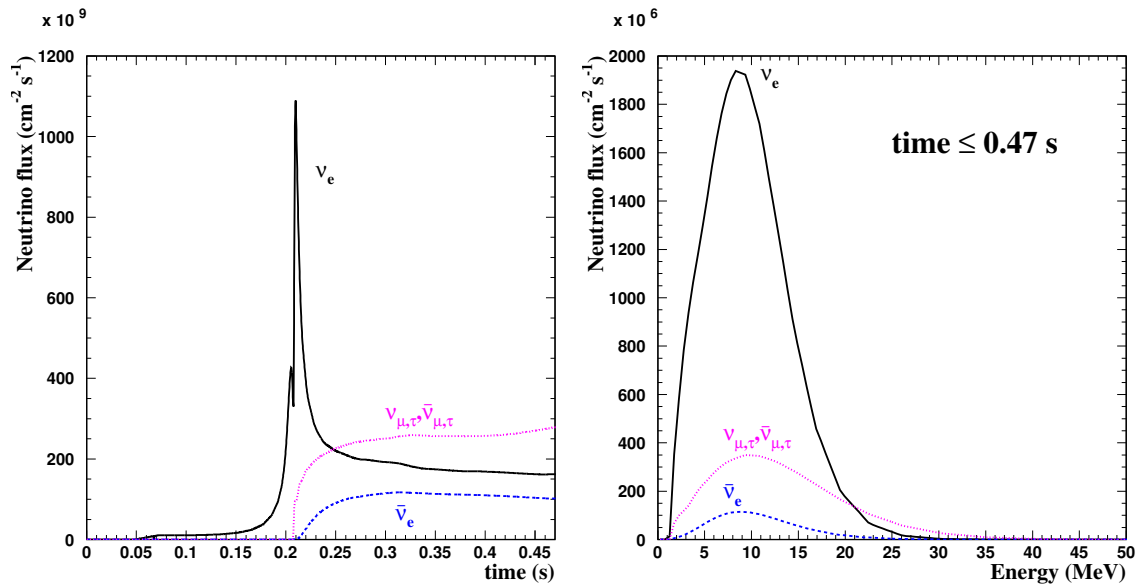


Figure 5: Evolution of the neutrino flux at Earth due to a neutrino burst from a supernova at a distance of 10 kpc. The time origin is arbitrary. On the right, time is integrated energy spectrum corresponding to the first 270 ms after the bounce.

CC process. This will allow to provide unique information about the early breakout pulse. But neutrino oscillations can however modify dramatically this situation. In the following we assume a normal mass hierarchy.

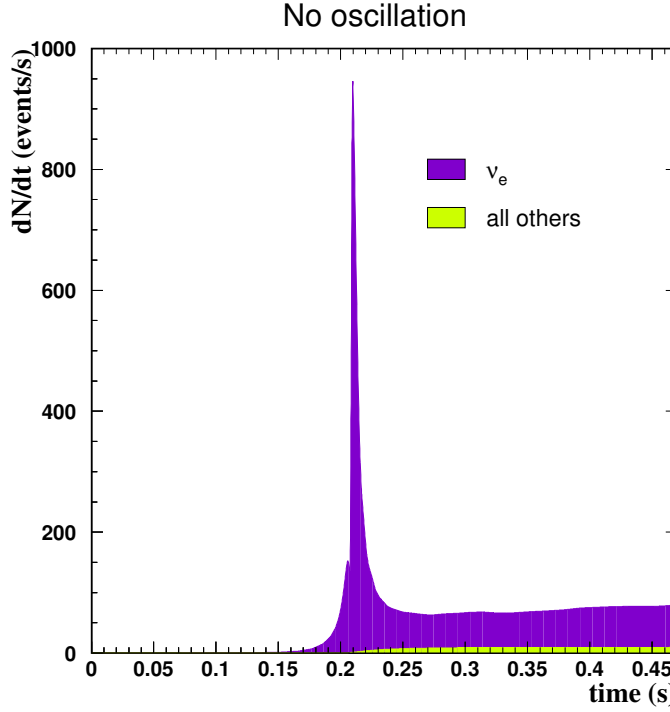


Figure 6: Expected neutrino event rates as a function of time in the 3 kton ICARUS detector. The dark region corresponds to the ν_e processes (elastic and CC) and the light region includes the contribution of the rest of flavors.

Figure 7 shows the two extreme oscillation cases depending on the value of the ν_{13} angle: the non adiabatic oscillation for small ν_{13} mixing angle (left) and the adiabatic oscillation for large ν_{13} values (right). For small ν_{13} the oscillation introduces a reduction of the ν_e peak. If the ν_{13} angle is large, the ν_e peak is sharply suppressed and essentially disappears due to the total conversion of ν_e into ν_τ .

Figures 8, 9, 10 and 11 contain the time evolution of the ν_e , ν_τ , ν_μ and $\bar{\nu}_e$ event rate expected in the 3 kton ICARUS detector for the first 270 ms after bounce and the corresponding time integrated event spectra. Since normal mass hierarchy is assumed here, the conversion in the antineutrino channel is always adiabatic and two cases (no oscillation and oscillation) are considered in the figures. On the other hand, the oscillation in the neutrino sector depends on the value of ν_{13} . Then, the two extreme cases (adiabatic and non adiabatic) are plotted together with the non oscillation possibility.

The reduction of the ν_e peak due to the effect of oscillations can be seen in figure 8. The suppression is maximal for adiabatic conversions. In contrast, a small ν_e peak appears as a consequence of the $\nu_e \rightarrow \nu_\tau$ conversion (figure 10). The energy spectrum

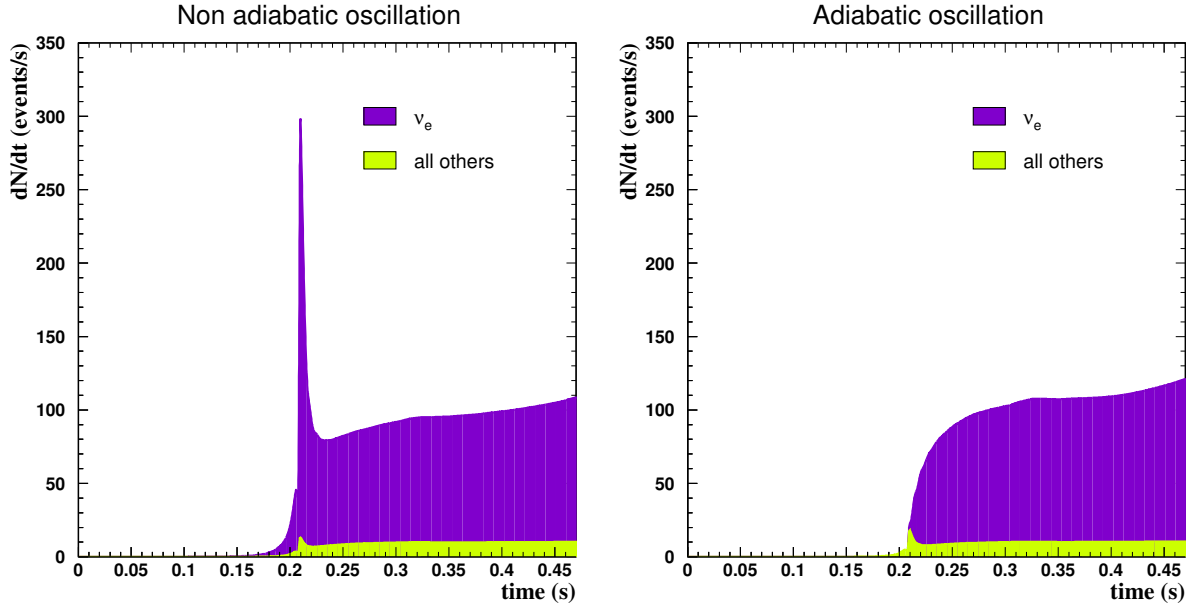


Figure 7: Time evolution of the event rates expected in the 3 kton ICARUS detector. Non adiabatic (left) and adiabatic (right) oscillation cases have been considered.

moves to lower neutrino energy values in this case. The situation in the antineutrino channels (figures 9 and 11) remains almost unchanged.

If we include oscillations, the expected number of ν_e events will be reduced. The integrated number of events as a function of time for the three cases (no oscillation, non adiabatic and adiabatic oscillations) is shown in figure 12. The ν_e events (CC and elastic interactions) are plotted for small and large ν_{13} mixing angle values with solid lines. The total contribution of the other flavors and interactions is indicated as dotted lines. The expected rates in the first milliseconds after the shock breakout are clearly dominated by the ν_e interactions in any case. This number increases with time and it depends on the ν_{13} value as indicated in figure 13. 10 events are expected in the first 40 ms after the shock breakout in case of no oscillations. The number of ν_e events is reduced to 4 events if we include oscillation effects for small ν_{13} mixing angle and it decreases for larger ν_{13} values down to 2 events.

5.1 Comparison between various cross-sections

In order to compute the event rates, the relevant nuclear cross-sections must be in principle known with relatively good precision from energies ranging from a few MeV up to 100 MeV.

In [6] the number of events from the breakout phase on Argon was computed with slightly more ν_e events than indicated by our results. This small difference can be readily attributed on the assumption made on the cross-section.

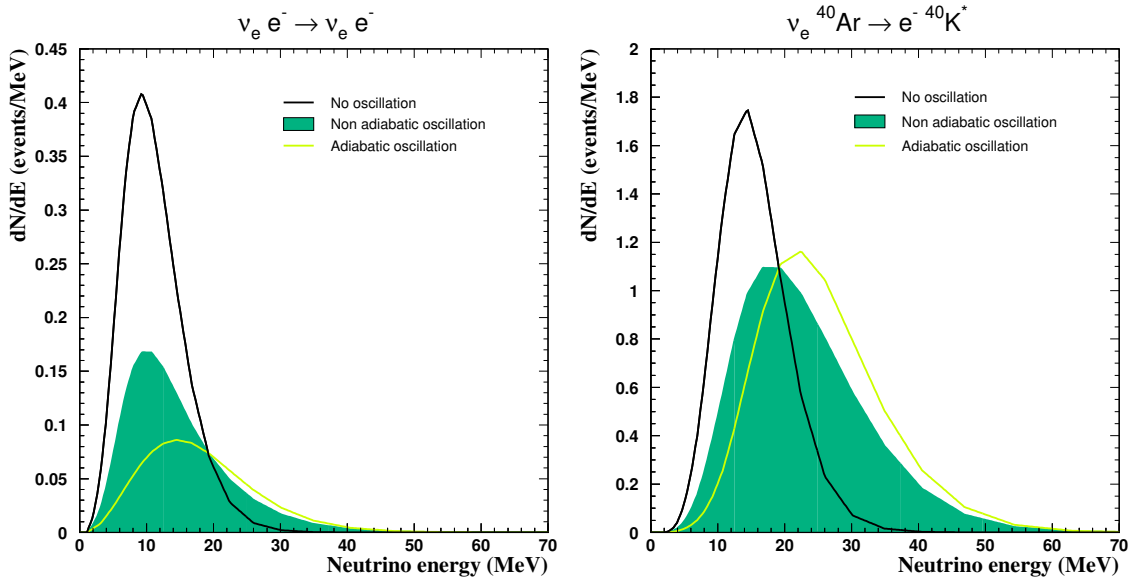
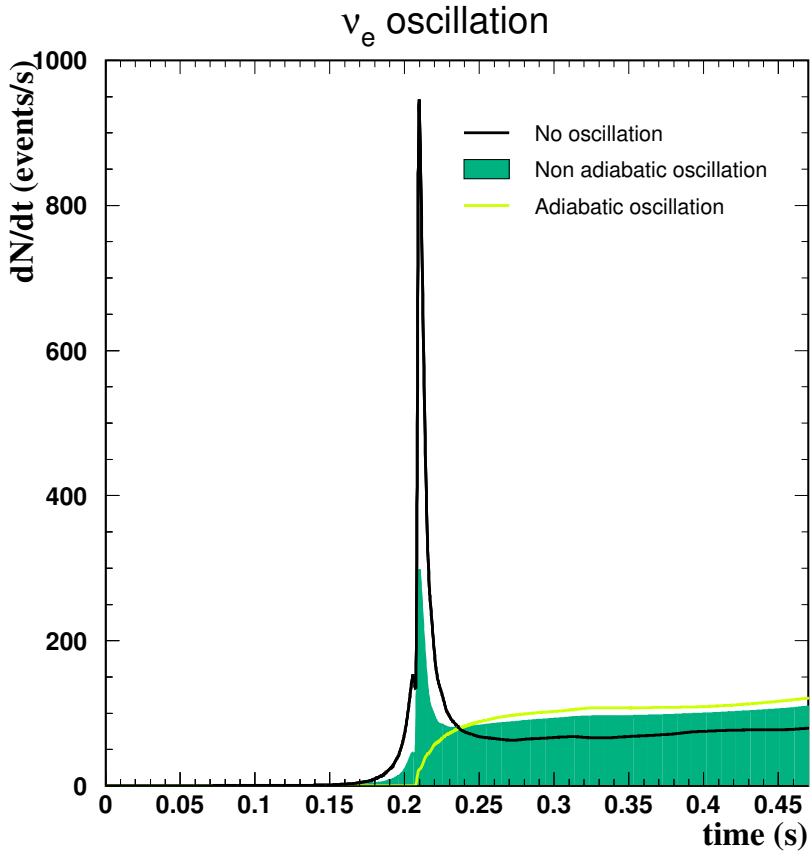


Figure 8: Time evolution of the ν_e event rate in ICARUS for the first milliseconds after the supernova bounce (top) and the corresponding time integrated event spectra for elastic and absorption processes (bottom). The no oscillation (dark curve), adiabatic (light curve) and non adiabatic (dark region) cases are considered.

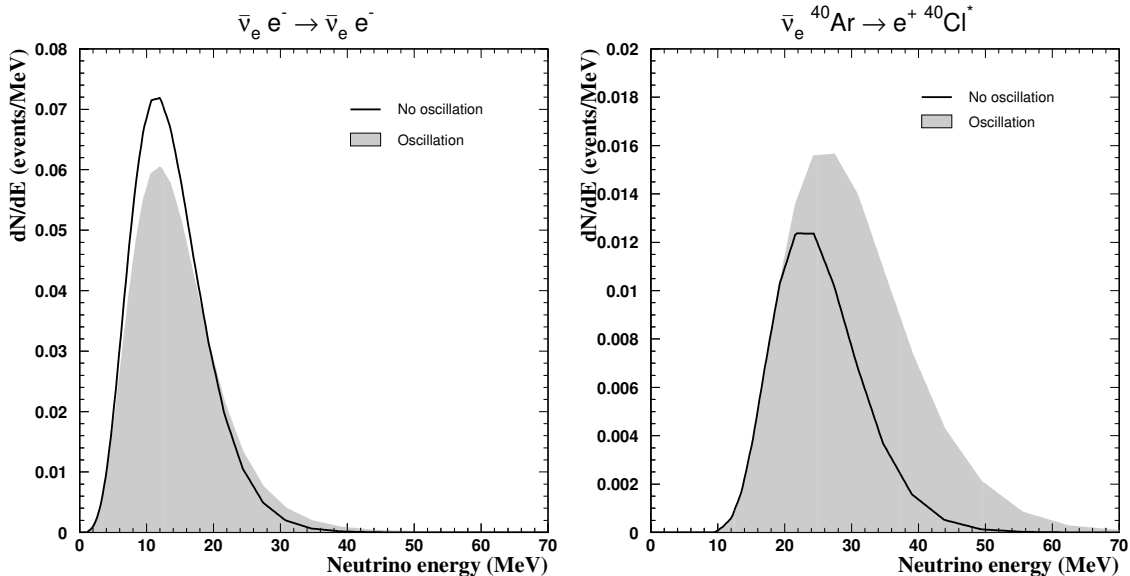
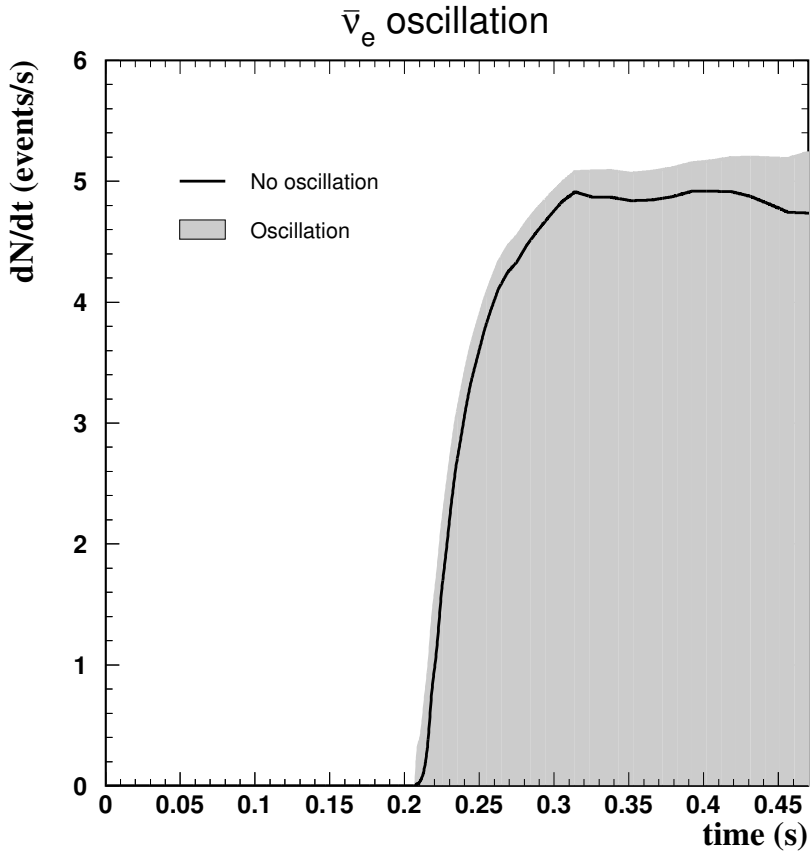


Figure 9: Time evolution of the ν_e event rate in ICARUS for the first milliseconds after the supernova bounce (top) and the corresponding time integrated event spectra for elastic and absorption processes (bottom). The non oscillation (dark line) and oscillation (gray region) cases are considered.

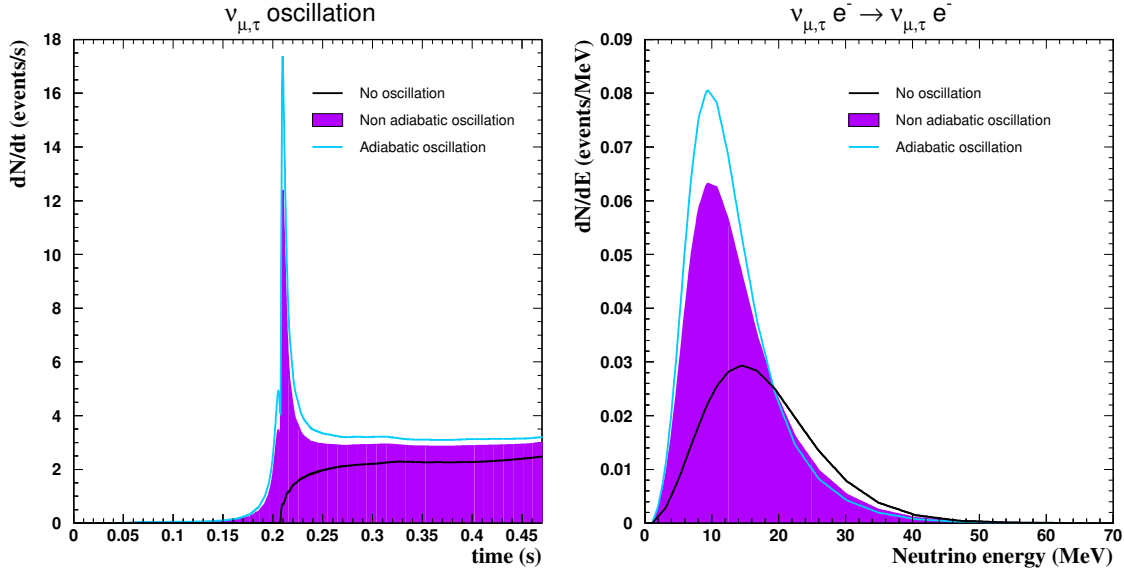


Figure 10: Time evolution of the $\nu_{\mu,\tau}$ event rate in ICARUS for the first milliseconds after the supernova bounce (left) and the corresponding time integrated event spectra for the elastic process (right). The no oscillation (dark curve), adiabatic (light curve) and non adiabatic (dark region) cases are considered.

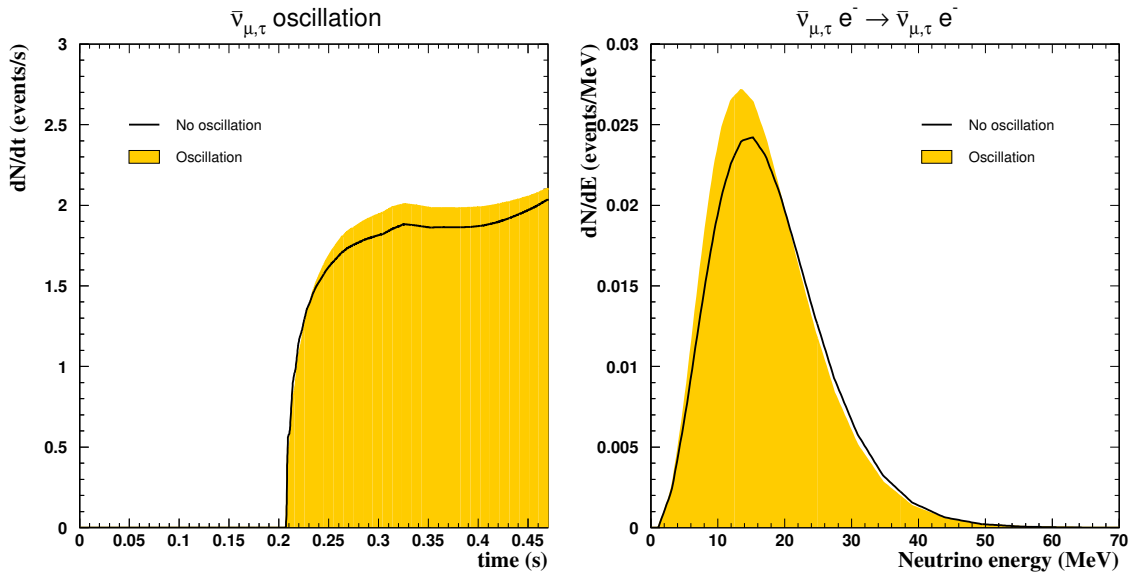


Figure 11: Time evolution of the $\nu_{\mu,\tau}$ event rate in ICARUS for the first milliseconds after the supernova bounce (left) and the corresponding time integrated event spectra for the elastic process (right). The no oscillation (dark line) and oscillation (gray region) cases are considered.

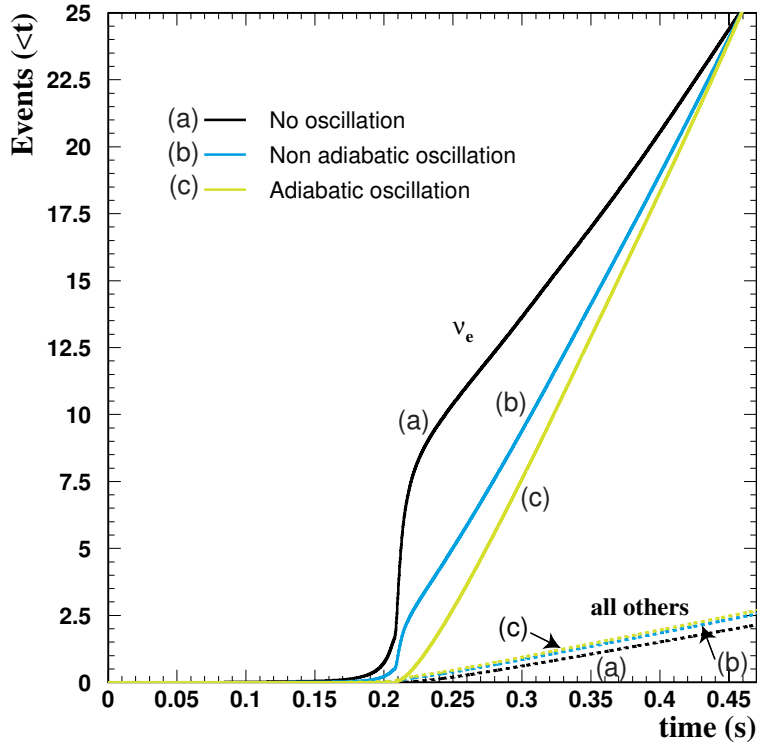


Figure 12: Time integrated number of events in ICARUS as a function of time for the first milliseconds after the supernova collapse. Solid lines correspond to ν_e neutrino interactions and dotted lines represent the rest of flavors interactions. Non oscillation, non adiabatic and adiabatic oscillation cases are considered separately.

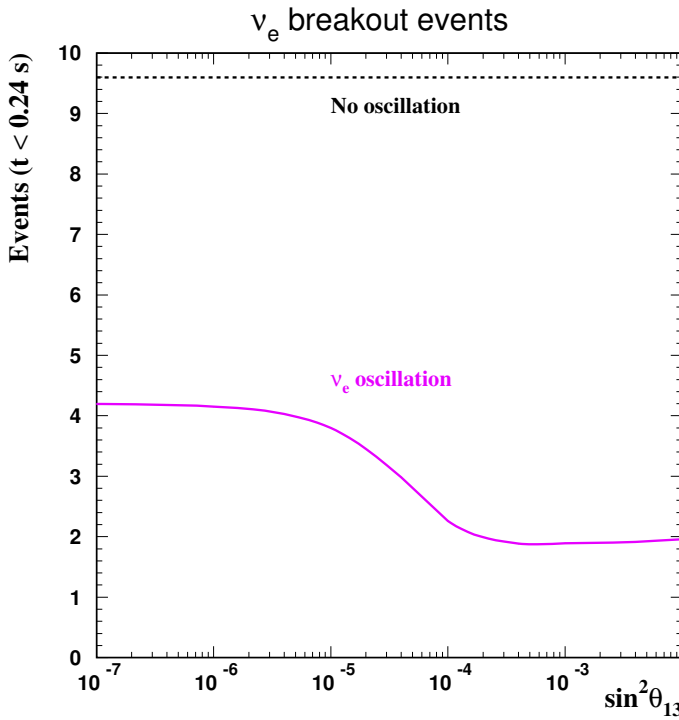


Figure 13: Expected ν_e events in ICARUS from the supernova shock breakout in the 40 ms after the supernova bounce. The solid line shows the variation of the number of events with the θ_{13} mixing angle. The dotted line corresponds to the expected number of events in case of no oscillations.

Figure 14 compares the cross section of the main neutrino interaction on Argon (e^- CC) computed in three different ways: the dashed line corresponds to the shell model calculations performed by Orm and [10] considering only Fermi and Gamow-Teller transitions. The dotted line is the assumption made in [6] where they take the total e^- absorption cross section as 3 times the cross section of the pure Fermi transition computed in [11]. Finally the solid line is the cross section used in this analysis that has been recently computed from Random Phase Approximation calculations including all possible multipoles [12]. We see that the assumption of $\sigma_{tot} = 3 \sigma_F$ overestimates the cross section for energies smaller than 30 MeV, which is the energy range of e^- from breakout.

The actual effect of the different cross section calculations can be checked in figure 15 where the time integrated number of e^- events is plotted as a function of time, for the first 270 ms after the shock breakout. We see that the Orm and RPA cross sections give similar results since in the energy range of the e^- neutrinos ($E < 30$ MeV) both calculations are equal. However, the approximation $\sigma_{tot} = 3 \sigma_F$ overestimates the expected number of events.

On the other hand, both Orm and $\sigma_{tot} = 3 \sigma_F$ cross sections underestimate the cross section for high energies up to 100 MeV, relevant for supernova neutrinos from the cooling phase (see section 6). The cross section including all the multipoles increases faster showing that not only the Fermi and Gamow-Teller transitions are important but also the rest of multipoles.

5.2 Comparison with other experiments

The integrated number of e^- events as a function of time for elastic and absorption processes without including oscillation effects are plotted in figure 16. The main contribution comes from the CC channel. Figure 17 shows similar plots for SuperKamiokande (SK) and SNO detectors.

The SK volume for supernova neutrino detection is 32 kton of light water. The dominant reaction is the charged-current absorption of e^- neutrinos on free protons ($e^- p \rightarrow e^- n e^+$). Neutrino scattering on electrons ($e^- \rightarrow e^-$) also contributes for all neutrino species. For the study of the shock breakout we calculate the event rates in SK due to only the e^- elastic scattering. For this process we use the neutrino-electron scattering cross section given in [8] with a threshold of 5 MeV. If there is large mixing angle between e^- and ν_μ or ν_τ neutrinos, the early e^- signal will be reduced significantly in SK.

The SNO detector is a light and heavy water neutrino detector containing 1 kton of D₂O surrounded by a cavity of 1.6 kton of light water. The main reactions for e^- neutrinos are the elastic scattering and the NC and CC reactions on deuterium ($e^- d \rightarrow e^- np$ and $e^- d \rightarrow ppe$). The cross sections used to compute these events are taken from [9].

Figure 18 shows the comparison between the expected number of events from the e^- burst in the three experiments. A total of 10 events are expected in the 3 kton ICARUS

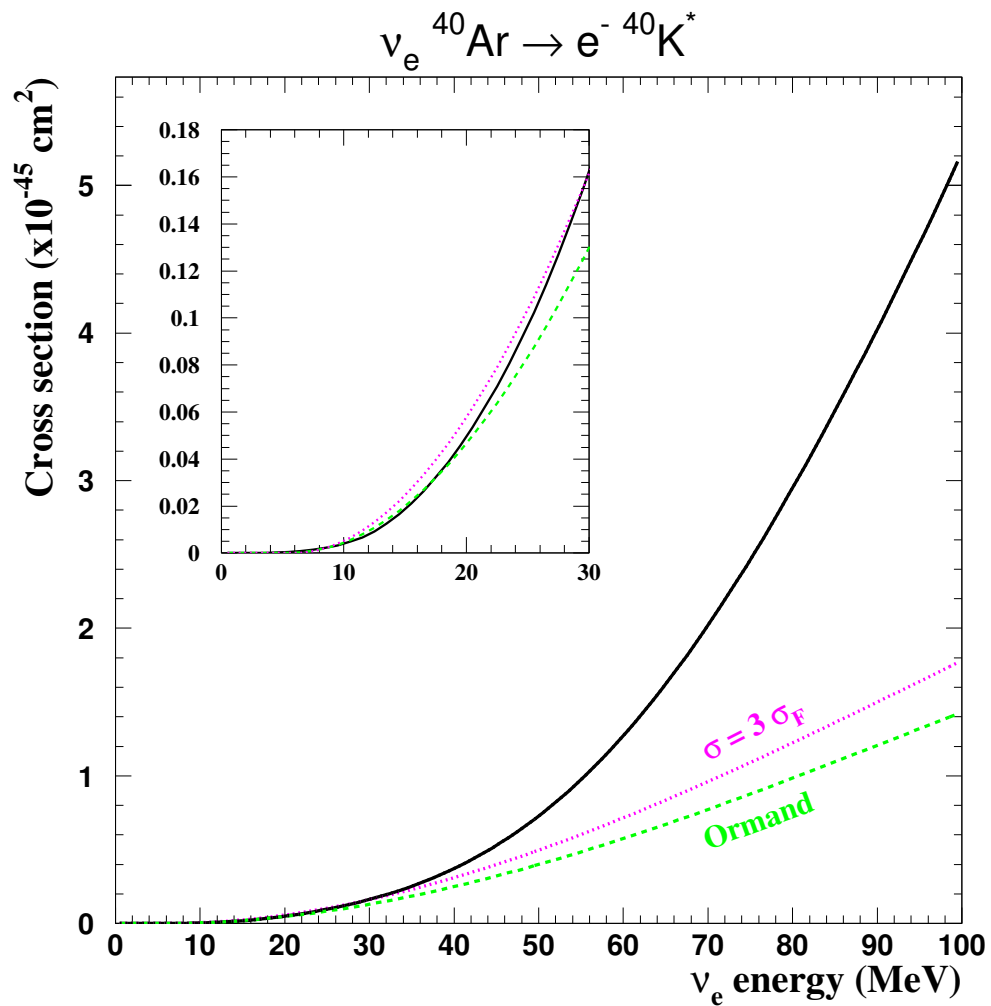


Figure 14: e^- CC cross section as a function of the neutrino energy. The dashed line corresponds to the Ormand and [10] cross section calculation, dotted line assumes that the total cross section of the absorption interaction is 3 times the cross section of the Fermi transition [6] and the solid line is the cross section used in this analysis calculated from RPA including all the transitions [12].

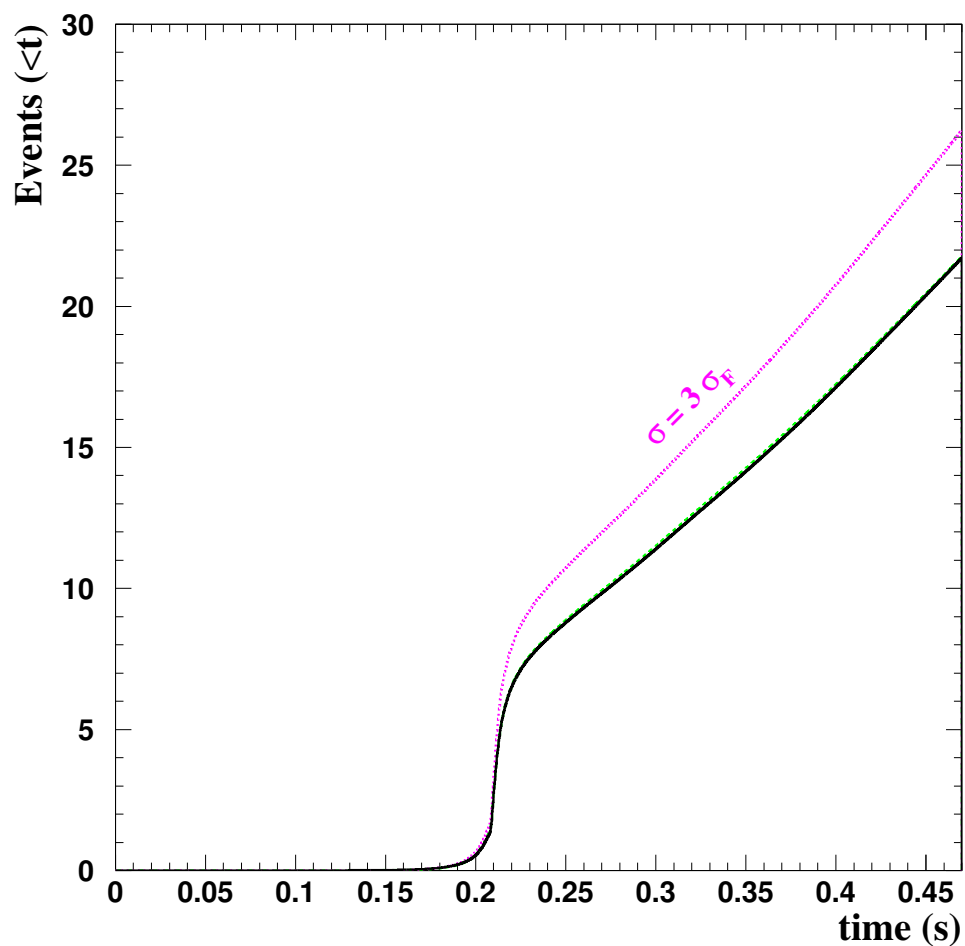


Figure 15: Time integrated number of ν_e events as a function of time for the first 270 ms after the shock breakout. We compare the results using the shell model calculations (dashed line [10]), the $\sigma_{tot} = 3\sigma_F$ approximation (dotted line) and the RPA calculations (solid line [12]).

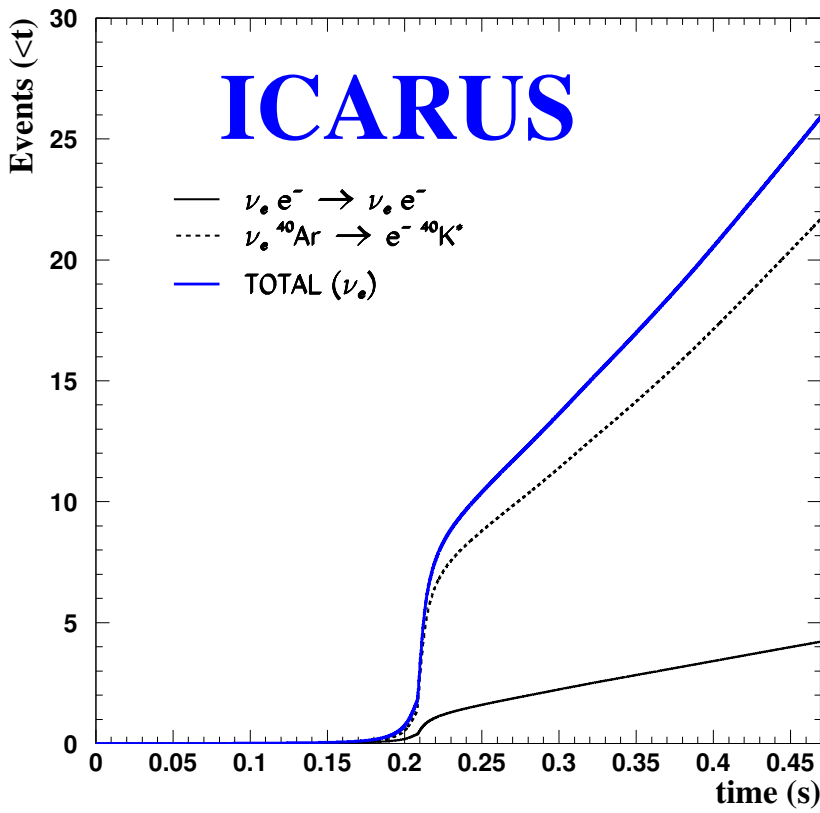


Figure 16: Integrated number of ν_e events as a function of time for the elastic and absorption channels. The thick solid line corresponds to the total number of events. No oscillation effects are included.

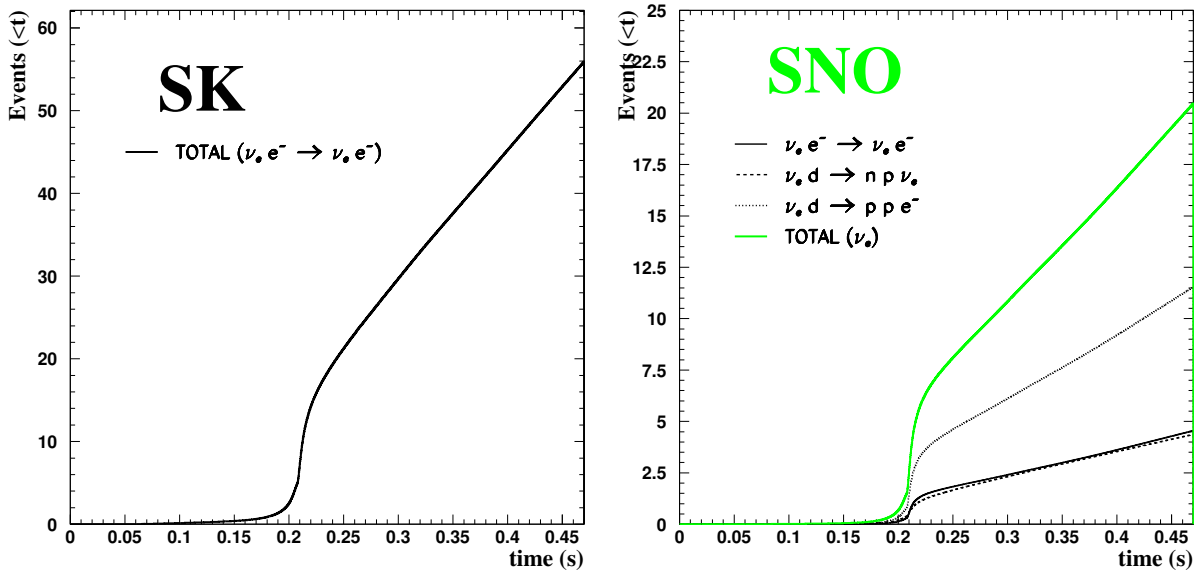


Figure 17: Integrated number of ν_e events as a function of time expected in the SK (left) and SNO (right) detectors. No oscillation effects are included.

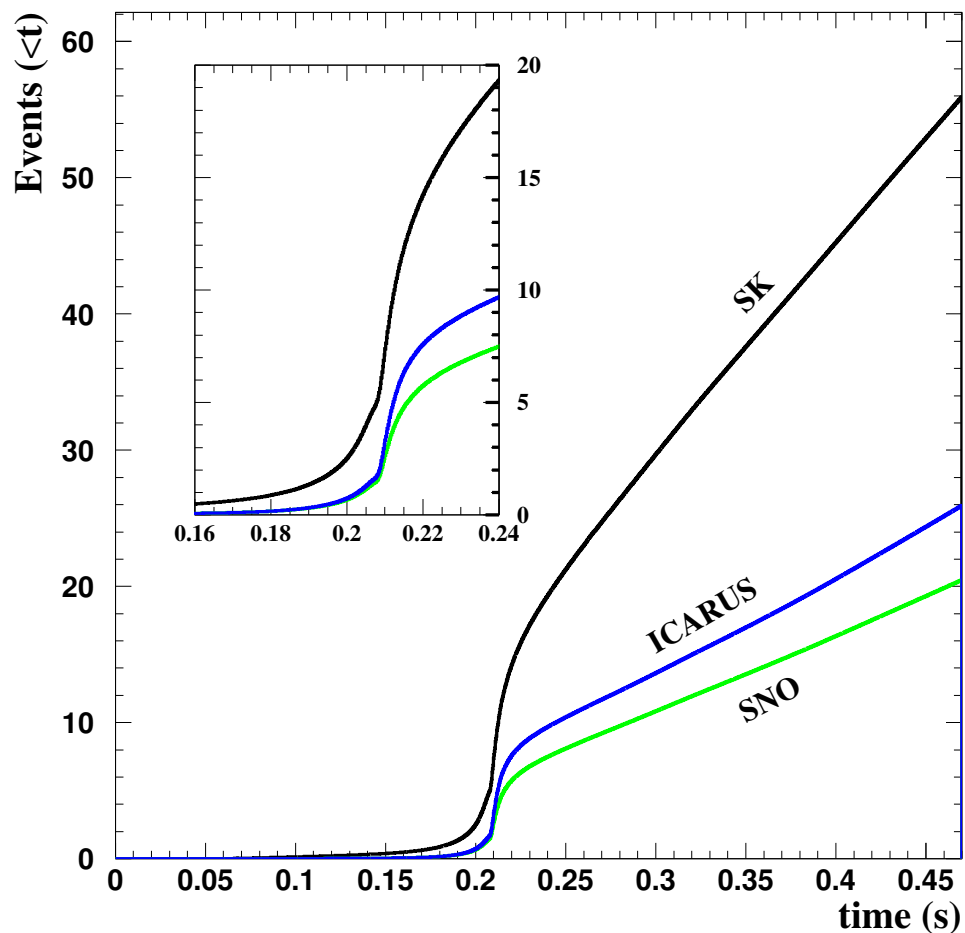


Figure 18: Comparison of the expected number of events from the ν_e breakout burst in ICARUS, SK and SNO experiments. In the first 40 ms after bounce a total of 20 events are expected in SK, 10 in ICARUS and 7 in SNO. No oscillation effects are included.

in the 40 ms after the bounce: 8 events from the absorption channel and 2 from the elastic channel. The contribution of SK and SNO for the same interval of time is 20 and 7 events, respectively.

6 Cooling phase

In this section we will refer to the main neutrino emission phase in the core collapse supernovae: the cooling of the star. 99% of its binding energy is radiated at this stage in form of all flavor neutrinos and antineutrinos.

As seen in previous sections, the energy spectra of the expected neutrinos at the detector will be modified by oscillations among flavors since the average neutrino energies are flavor dependent and the interaction cross sections are different for different flavors. The variations of the neutrino energy will depend on the adiabaticity conditions on the H and L resonances in the supernova and on the neutrino oscillation parameters.

Four different cases corresponding to different oscillation conditions are considered in this analysis depending on the type of mass hierarchy and the value of the $_{13}$ mixing angle: n.h.-L (normal hierarchy and large $_{13}$), n.h.-S (normal hierarchy and small $_{13}$), i.h.-L (inverse hierarchy and large $_{13}$) and i.h.-S. (inverse hierarchy and small $_{13}$).

Table 1 contains the number of neutrino events from a supernova at 10 kpc expected in the 3 kton ICARUS detector. Elastic and absorption processes have been considered independently and oscillation and non oscillation cases have been computed for normal and inverted hierarchies. Although only the two extreme cases of the $_{13}$ value are included in the table, we are able to compute the explicit dependence of the rates with the angle $_{13}$, as will be explained in section 6.1.

Reaction	Expected events in 3 kton ICARUS					
	No oscillation	Oscillation (n.h.)		Oscillation (i.h.)		
		Large $_{13}$	Small $_{13}$	Large $_{13}$	Small $_{13}$	
Elastic						
$e^- e^-$	20	20	20	20	20	20
$e^- e^-$	8	8	8	8	8	8
$(\mu^- + \tau^-) e^-$	7	7	7	7	7	7
$(\mu^- + \tau^-) e^-$	6	6	6	6	6	6
total e^-	41	41	41	41	41	41
Absorption						
CC	$e^- {}^{40}\text{Ar}$	188	962	730	730	730
	$e^- {}^{40}\text{Ar}$	15	33	33	75	33
Total		244	1036	804	846	804

Table 1: Expected neutrino events in the 3 kton ICARUS detector from a supernova at a distance of 10 kpc including neutrino oscillations with matter effects inside the supernova (no threshold on the electron energy has been applied).

Figures 19, 20 and 21 show the effect of the oscillations in the neutrino energy spectra. The different neutrino reactions are plotted separately. The plots on the top correspond to the expected number of neutrinos arriving at Earth and the bottom plots are the corresponding number of events detected in ICARUS. The four oscillation cases are considered in the distributions.

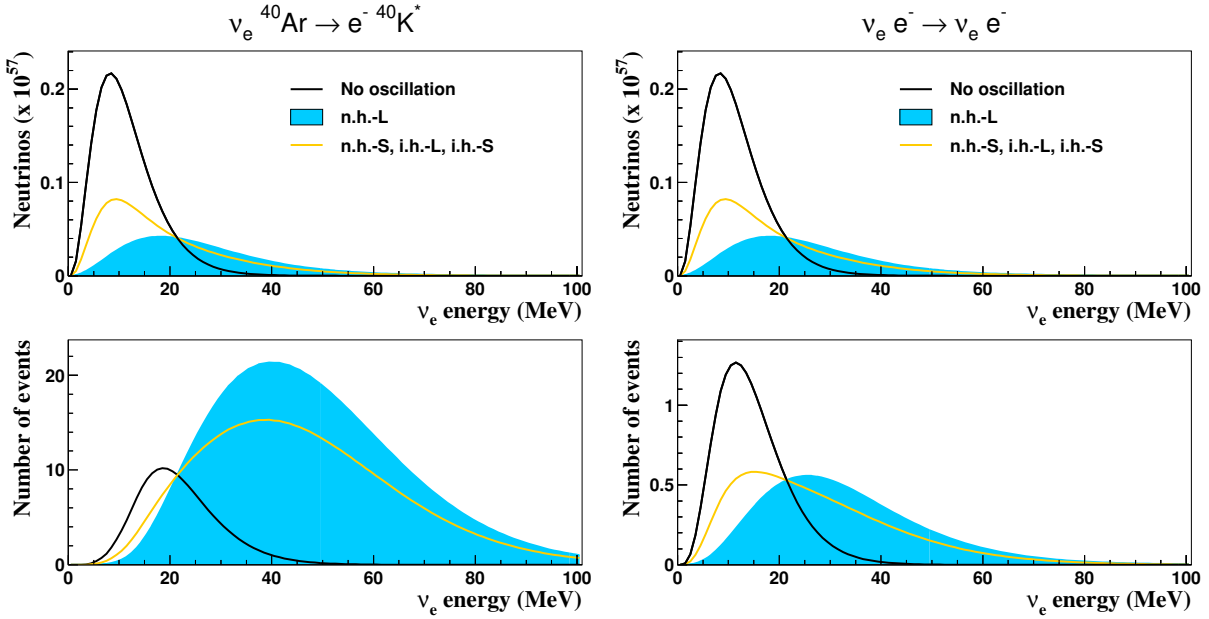


Figure 19: Number of neutrinos arriving at Earth (top) and expected number of events in the 3 kton ICARUS detector (bottom) for ν_e neutrinos from a supernova at 10 kpc. The non oscillation and the four oscillation cases have been taken into account. The CC interaction process (left) and elastic scattering (right) are split in the figure.

As was mentioned in section 3, normal and inverted hierarchies are degenerated for small $_{13}$ in all the cases. In the neutrino (antineutrino) channel and i.h. (n.h.) the conversion is adiabatic and results are independent on $_{13}$. Maximum conversion occurs for large mixing angle in the neutrino (antineutrino) channel for n.h. (i.h.).

Note that the ν_e ux and $\bar{\nu}_e$ ux have essentially different information about the neutrino oscillation parameters. For example, i.h.-L and i.h.-S are distinguishable from ν_e events but are not from $\bar{\nu}_e$ events. Then, a good separation of these events is desirable in order to distinguish between models.

Due to the total conversion $\nu_e \rightarrow \bar{\nu}_e$ for the n.h.-L case, the ν_e energy spectra is harder and this leads a huge increase of the expected events due to the quadratic dependence of the CC cross section with energy. The same effect can be seen for ν_e events and i.h.-L case. The elastic processes are less sensitive to the oscillations and smaller number of events is expected. Nevertheless, the energy spectrum is modified specially for ν_e events, moving to lower values of energy due to the neutrino mixing.

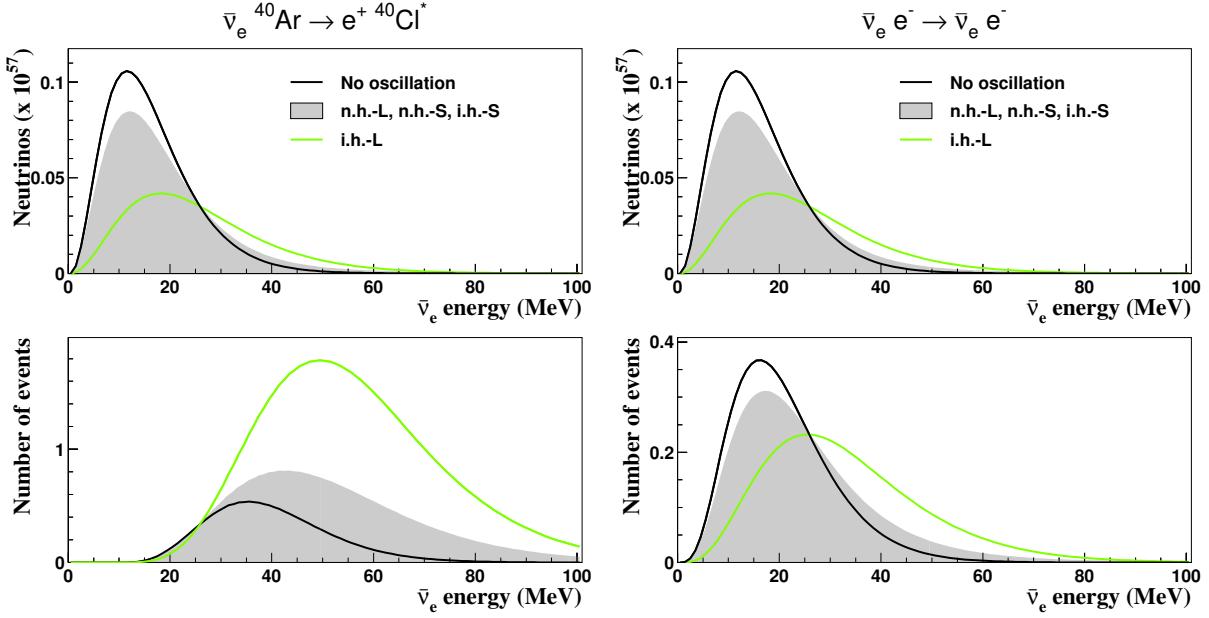


Figure 20: Number of neutrinos arriving at Earth (top) and expected number of events in the 3 kton ICARUS detector (bottom) for $\bar{\nu}_e$ neutrinos from a supernova at 10 kpc. The non oscillation and the four oscillation cases have been taken into account. The CC interaction process (left) and elastic scattering (right) are split in the figure.

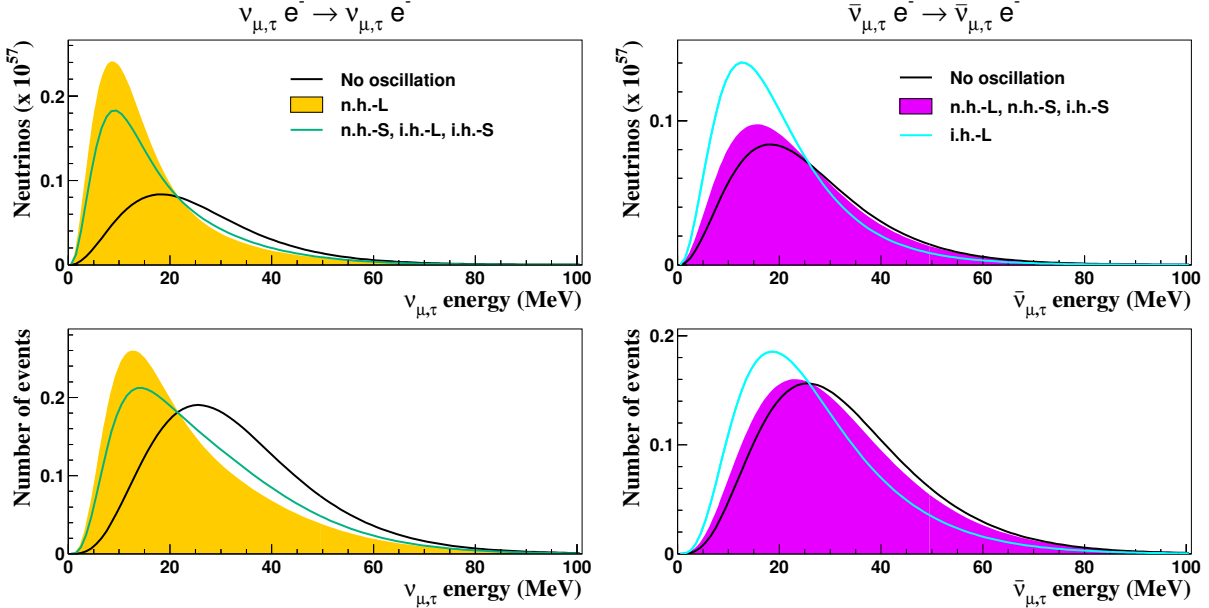


Figure 21: Number of neutrinos arriving at Earth (top) and expected number of events in the 3 kton ICARUS detector (bottom) for $\nu_{\mu,\tau}$ (left) and $\bar{\nu}_{\mu,\tau}$ (right) neutrinos from a supernova at 10 kpc. The non oscillation and the four oscillation cases have been taken into account.

6.1 Dependence on the θ_{13} angle

The explicit variation of the expected rates and energy spectra with the θ_{13} angle can be computed considering the dependence of the jump probability with this angle (section 3).

Figure 22 shows for all the neutrino flavors the expected number of neutrinos arriving at Earth as a function of $\sin^2 \theta_{13}$. We compare the non oscillated and oscillated cases assuming normal mass hierarchy. There is no variation of the expected rates as a function of the mixing angle in the antineutrino sector. However, the neutrino sector is sensitive to this parameter, specially in the intermediate range. We can distinguish the three regions we mentioned before.

Considering the cross sections corresponding to every process, we compute the variation of the neutrino rates expected in ICARUS as a function of $\sin^2 \theta_{13}$. We compare the expected results with (solid line) and without (dotted line) oscillations assuming normal mass hierarchy. CC events are very sensitive to the change on the energy spectra due to oscillations. A clear increase on the number of events is expected, being of a factor (4{5) for e CC events and a factor 2 for e CC interactions. The main variations with the angle θ_{13} are expected for the e channels, specially for CC events. The number of events increases 30% from small to large θ_{13} values. Small variations are expected for the rest of channels.

Although the number of events does not change, the energy spectra are affected by oscillations and in particular by the value of the θ_{13} angle. This can be seen in figures 24, 25 and 26, where the energy spectra of e , e and μ , μ , are plotted for different values of $\sin^2 \theta_{13}$ and different reactions. Only the normal hierarchy case is plotted.

The conversion is always adiabatic in the antineutrino sector for normal hierarchy. Therefore, there is no dependence with θ_{13} . For the neutrino channels, we can see the variation of the spectrum between the two extreme values of θ_{13} . The effect is specially important for e CC events. Information about this angle can be obtained from these distributions.

7 Conclusions

We have performed an analysis of the neutrino events expected in a liquid Argon TPC (ICARUS-like) from a future galactic supernova has been performed showing the high capabilities of the detector to observe neutrinos from stellar collapses and extract information about their properties.

In a previous paper we have considered three detection channels: elastic scattering on electrons from all neutrino species, e charged current absorption on Ar with production of excited K and e charged current absorption on Ar with production of excited C 1. The present work includes a detail study of the dependence with the mixing angle θ_{13} and the type of mass hierarchy. For definiteness we assumed the 3kton ICARUS detector and a supernova at a distance of 10 kpc.

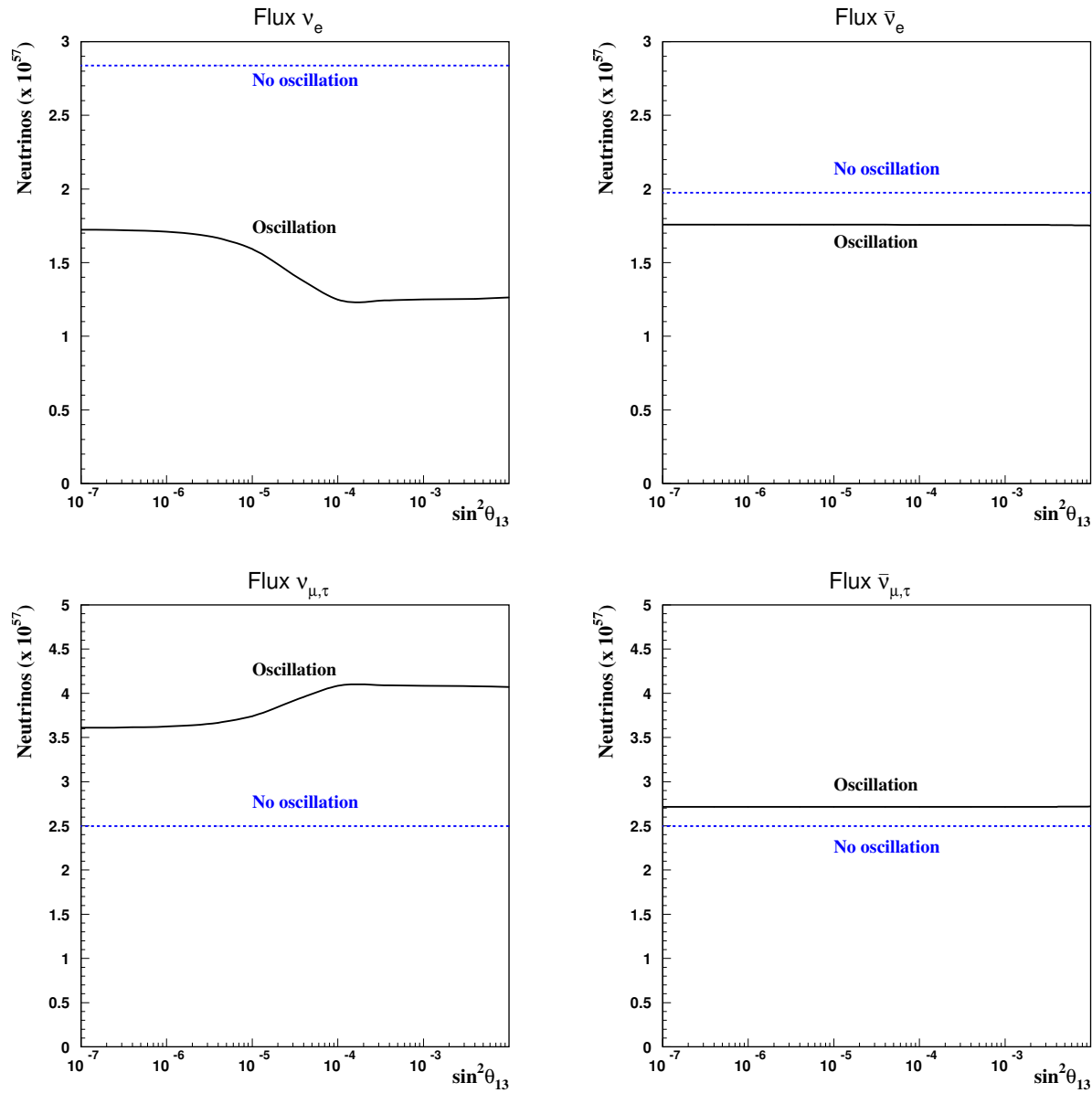


Figure 22: Expected number of neutrinos arriving at Earth as a function of $\sin^2 \theta_{13}$. The dotted line corresponds to the non oscillation case and the solid line represents the variation of the number of neutrinos considering oscillations.

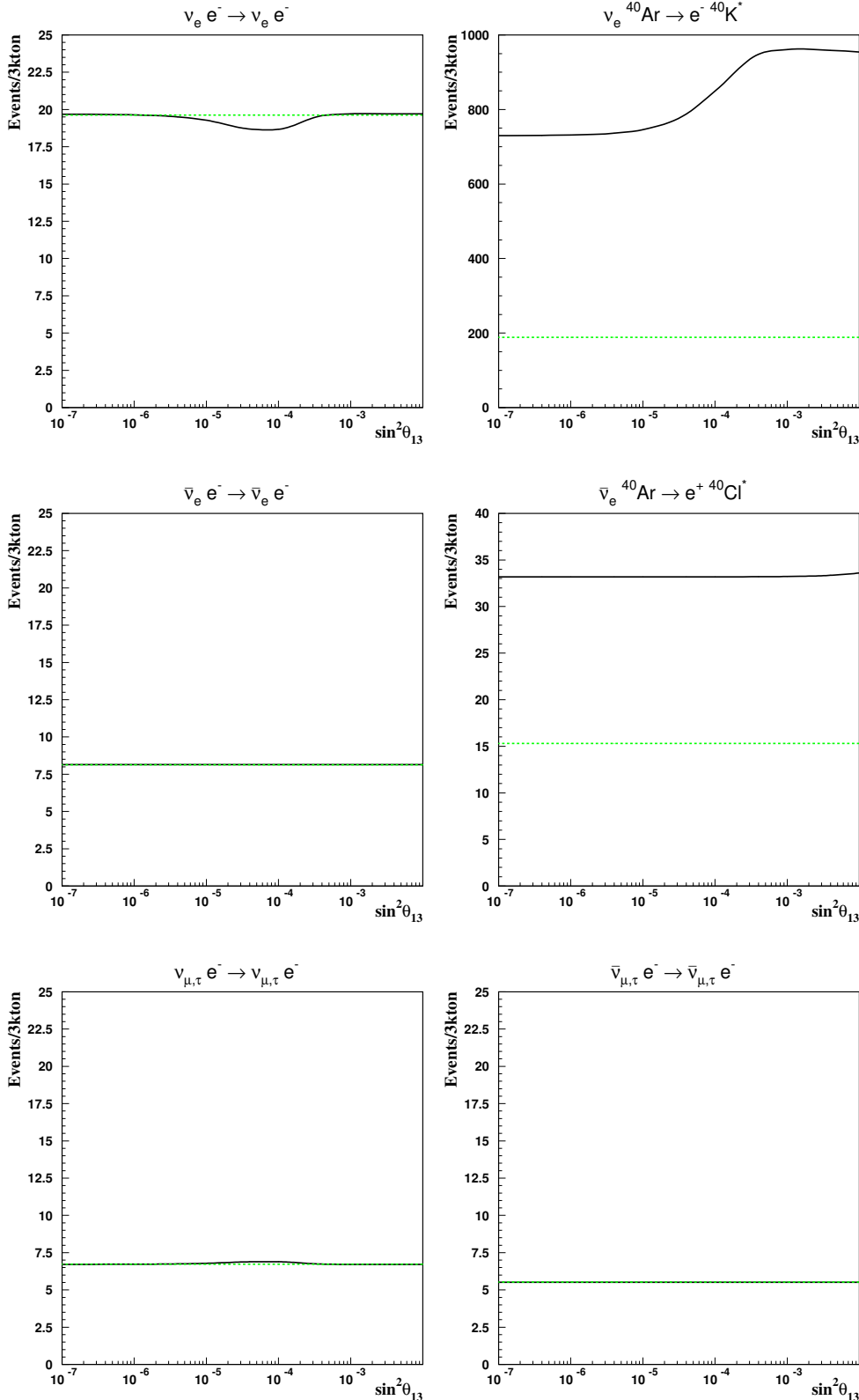


Figure 23: Expected number of events in a 3 kton ICARUS detector as a function of $\sin^2 \theta_{13}$. The different neutrino interaction processes for every neutrino flavor expected in ICARUS are plotted separately. Solid lines correspond to the oscillation case and dotted lines to the non oscillation case.

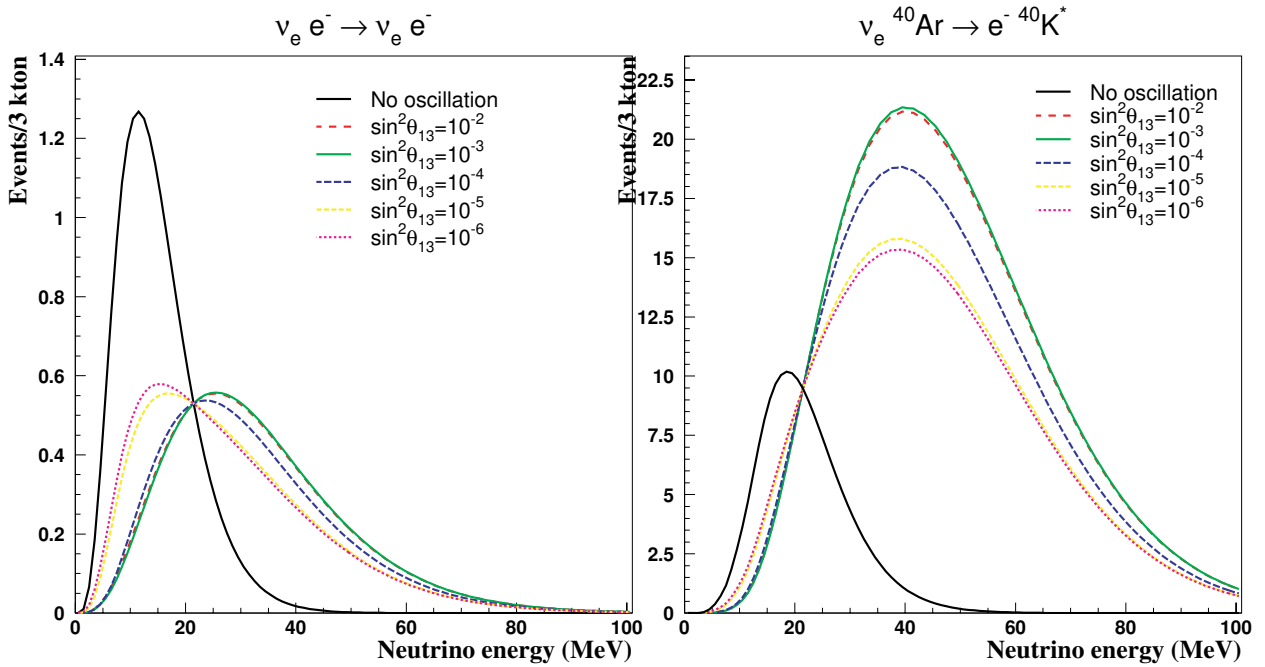


Figure 24: Energy spectra of expected ν_e events in ICARUS coming from a supernova at 10 kpc. Different values of $\sin^2 \theta_{13}$ are considered for charged-current (right) and elastic (left) processes.

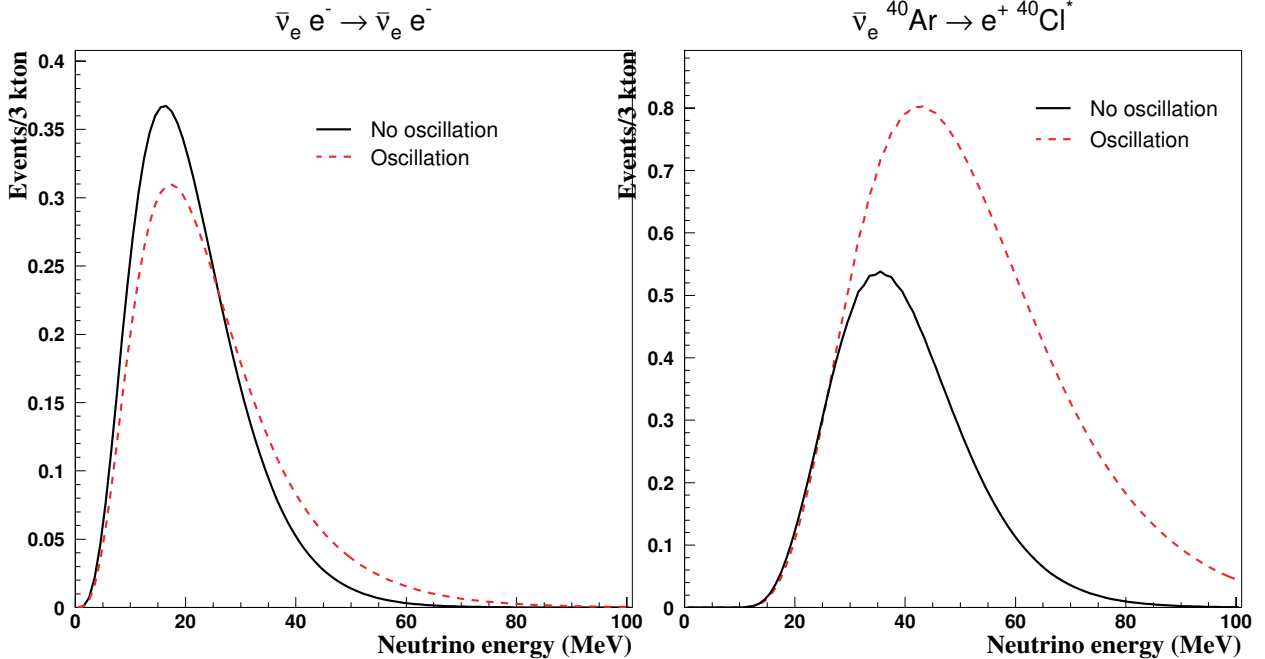


Figure 25: Energy spectra of expected ν_e events in ICARUS coming from a supernova at 10 kpc. No oscillation and oscillation cases are considered for charged-current (right) and elastic (left) processes.

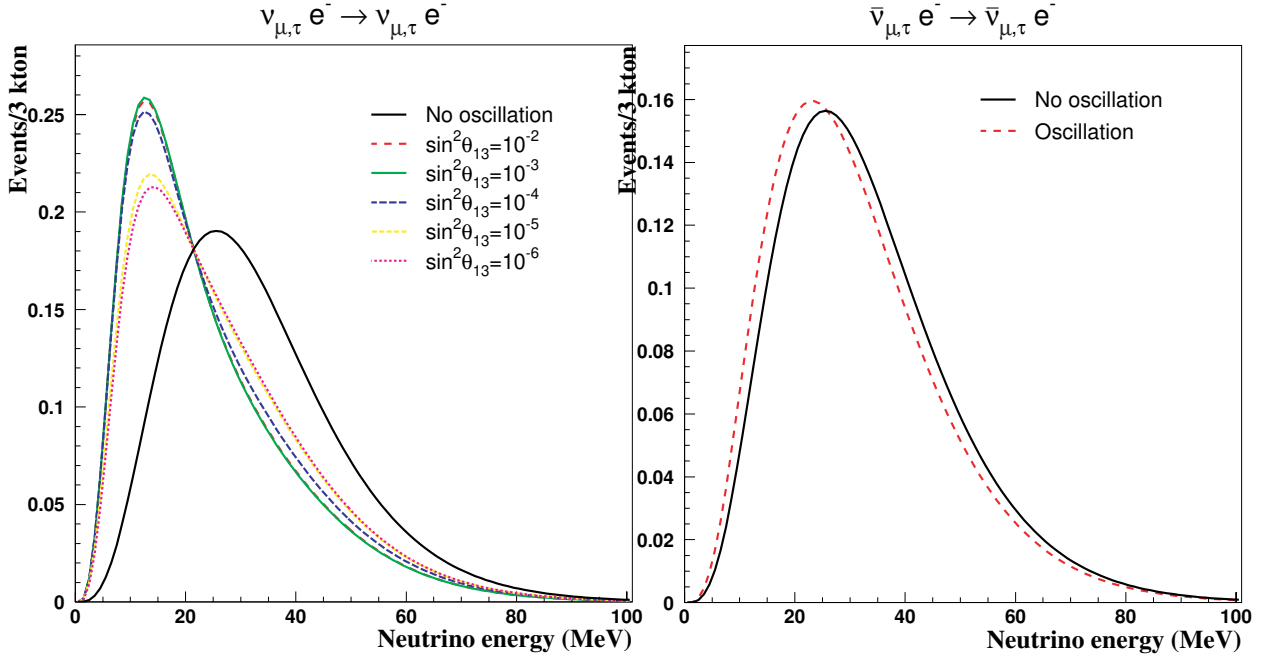


Figure 26: Energy spectra of expected $\nu_{\mu,\tau} e^- \rightarrow \nu_{\mu,\tau} e^-$ (left) and $\bar{\nu}_{\mu,\tau} e^- \rightarrow \bar{\nu}_{\mu,\tau} e^-$ (right) elastic events in ICARUS coming from a supernova at 10 kpc. Different values of $\sin^2 \theta_{13}$ are considered for the $\nu_{\mu,\tau} e^-$ elastic channel.

Neutrino oscillations change significantly the expected supernova neutrino rates and energy spectra. The matter effects inside the supernova must be included to know how the spectra of the neutrino burst is modified by oscillations.

Information about the supernova explosion mechanism can also be obtained from the study of the neutrino burst coming in the first milliseconds after the supernova collapse. The early phase neutrino signal from supernova has been studied using a realistic core collapse supernova model [6], including oscillation effects. Thanks to its clean identification and high sensitivity to ν_e neutrinos, a liquid Argon TPC can provide fundamental information about the shock breakout mechanism.

A set of observables sensitive to the supernova neutrino parameters and to the intrinsic neutrino oscillation parameters (θ_{13} and mass hierarchy) must be defined in order to be able to distinguish between the different oscillation scenarios and to fix the supernova parameters. In order to understand more precisely the sensitivity to such effects, one should study the classification of actual detected events into the three channels: ν_e elastic, ν_e charged current and ν_e charged current.

In addition, since neutrinos can go through the Earth before reaching the detector, the matter effects inside the Earth can change the neutrino spectra again. Using a realistic Earth density profile, new calculations on the neutrino spectra can be performed.

An analysis taking into account all these effects will be the subject of a future work.

Acknowledgments

We would like to acknowledge T. A. Thompson and A. Burrows for providing data about the neutrino breakout spectra of core collapse supernovae and for useful discussions.

References

- [1] K. Hirata et al., *Phys. Rev. D* 38 (1988) 448; *Phys. Rev. Lett.* 58 (1987) 1490.
R. Bionta et al., *Phys. Rev. Lett.* 58 (1987) 1494.
- [2] S. Fukuda et al., *Phys. Rev. Lett.* 86 (2001) 5656.
SNO Collaboration, *Phys. Rev. Lett.* 87 (2001) 071301.
Y. Fukuda et al., *Phys. Rev. Lett.* 82 (1999) 2644.
KamLAND Collaboration, *Phys. Rev. Lett.* 90 (2003) 021802.
M. Apollonio et al., *Phys. Lett. B* 466 (1999) 415.
K2K Collaboration, *Phys. Rev. Lett.* 90 (2003) 041801.
- [3] A. Bueno, I. G. Iacobella and A. Rubbia, "Supernova Neutrino Detection in a liquid Argon TPC", [hep-ph/0307222](http://arxiv.org/abs/hep-ph/0307222).
- [4] ICARUS Collab., "ICARUS. A Second-Generation Proton Decay Experiment and Neutrino Observatory at the Gran Sasso Laboratory", all proposals are available at <http://www.cern.ch/icarus>.
- [5] A. S. Dighe and A. Y. Smirnov, *Phys. Rev. D* 62 (2000) 033007.
- [6] T. A. Thompson, A. Burrows and P. A. Pinto, "Shock Breakout in Core-Collapse Supernovae and its Neutrino Signature", [astro-ph/0211194](http://arxiv.org/abs/astro-ph/0211194), submitted to *Astrophys. J.*, 2002.
- [7] K. Takahashi, K. Sato, A. Burrows and T. A. Thompson, "Supernova Neutrinos, Neutrino Oscillations and the Mass of the Progenitor Star", [hep-ph/0306056](http://arxiv.org/abs/hep-ph/0306056).
- [8] Y. Totsuka, *Rep. Prog. Phys.* 55 (2002) 377.
- [9] S. Nakamura et al., *Nucl. Phys. A* 707 (2002) 561.
S. Ying, W. C. Haxton and E. M. Henley, *Phys. Rev. D* 40 (1989) 3211.
- [10] W. E. Ormand, P. M. Pizzochero, P. F. Bortignon and R. A. Broglia, *Phys. Lett. B* 345 (1995) 343 [[nucl-th/9405007](http://arxiv.org/abs/nucl-th/9405007)].
- [11] R. S. Raghavan, *Phys. Rev. D* 34 (1986) 2088.
- [12] G. Martínez-Pinedo, E. Kolbe and K. Langanke (private communication).